Important Information

This document is an English translation of the original Bachelor's thesis originally written in Polish, which was a formal requirement of the university. The translation was performed chapter-by-chapter by the AI model **Gemini Thinking** on **December 25, 2025**.

Please be advised that this English version has undergone only a brief review; therefore, linguistic inaccuracies or translation errors may occur. The formal academic review and defense process applied exclusively to the original Polish version. Additionally, some figures and tables may remain in their original language.

This version has been created solely for the purpose of sharing the research findings. I remain open to any questions regarding the content.

Wrocław University of Science and Technology
Faculty of Electronics, Photonics and Microsystems

Field of Study: System Controll and Robotics Engeneering

BACHELOR THESIS

Title of Thesis:
Steering algorithms of floating robots

Author:
Antoni Piałucha

Supervisor:
dr inż. Mateusz Cholewiński

WROCŁAW 2025

Abstract

This thesis addresses the issues of control and navigation of Unmanned Surface Vehicles (USV). The theoretical part reviews design solutions for marine robots and presents a kinematic model of a vessel with three degrees of freedom (3 DOF). The research platform utilized, the differential-drive "FOKA" robot, is also described. A significant part of the thesis involves the analysis of navigation methods, covering classical, dead reckoning, and hybrid approaches. The control layer section presents the implementation of a differential drive algorithm. An azimuth control system for point-to-point navigation was developed, and two types of trajectory tracking controllers were implemented: ILOS (*Integral Line-of-Sight*) and PID, both designed to compensate for steady-state errors caused by environmental disturbances. The controller tuning process and the verification of navigation and control algorithm effectiveness were conducted in the Gazebo Sim (gz sim) simulation environment. The work concludes with experiments on the physical platform, confirming the effectiveness of the azimuth stabilization algorithm in real-world conditions.

Keywords: USV, marine robots, differential drive, navigation, ILOS, ROS 2, Gazebo Sim

Contents

Chapter 1

Introduction

Since the dawn of time, water has been a fundamental element of human existence, conditioning biological survival, the success of crops, and civilizational development. For millennia, it has also served as a key communication route. The oldest indirect evidence of the use of watercraft by early hominins consists of stone tools found on the Indonesian island of Sulawesi. These artifacts date back at least one million years, falling within the Early Pleistocene. Given that even with lowered sea levels during glaciations, these areas remained separated from the mainland by deep waters, the presence of human ancestors in this region indicates the necessity of using means of transport capable of crossing sea straits [7]. In turn, the oldest direct evidence of shipbuilding, physically preserved to modern times, is the Pesse canoe (Netherlands). This dugout, made from a single trunk of Scots pine, dates back to approximately 8000 BC and originates from the Mesolithic period [23]. Its photograph is presented in Figure 1.1.

Nowadays, maritime transport constitutes the foundation of the global economy, relying primarily on vessels with a displacement of hundreds of thousands of tons, such as container ships or passenger ferries. Until recently, the use of smaller units was mainly limited to recreational purposes; however, this situation is undergoing a dynamic change due to progress in the fields of robotics and automation. A traditional boat, designed for multi-month sea missions, had to have dimensions that provided facilities for a multi-person crew. The elimination of the human factor allows for significant miniaturization and an operational paradigm shift. Currently, companies such as Ocean Infinity are deploying fleets of autonomous units capable of scanning vast ocean areas without direct human involvement. Unmanned Surface Vehicles (USV) are also utilized in the investigation of hazardous areas, such as damaged hydro-technical infrastructure or chemically contaminated reservoirs, for example, post-flotation tailings ponds near mines.

Control and navigation algorithms are an indispensable element of the operation of both large-scale and smaller autonomous units. Although their specifics depend strictly on the hull design, the propulsion system configuration, and the mission profile, many challenges remain universal for this entire class of objects. These include, among others, positioning, trajectory tracking, and ensuring the robustness of the control system against environmental disturbances, such as varying wind or wave action.

1.1 Aim and Scope of the Thesis

The main objective of this thesis is the development, implementation, and verification of control algorithms for a floating robot of the USV class. This research encompasses both

Figure 1.1: The Pesse canoe found in the Netherlands (approx. 8000 BC) [9].

numerical simulations and real-world tests on a selected research object. Achieving this goal required a series of analytical and engineering actions. First, a literature review of ship control methods was conducted, which allowed for the selection of appropriate theoretical solutions. Subsequently, a mathematical model of the object was developed, which is essential for conducting reliable simulations. The next stage involved the implementation of selected control algorithms in a programming environment. The work concluded with experiments verifying the adopted assumptions and an evaluation of the control quality in specified test scenarios.

Chapter 2

Overview of Floating Robots

Unmanned surface vehicles (USVs) can be divided into several basic design categories, which differ in the propulsion systems used, maneuvering characteristics, and the level of complexity regarding integration with autonomous systems. Two main groups of solutions are most commonly encountered.

The first group consists of units utilizing propulsion systems where the direction of the thrust force is controlled independently of its magnitude. This is typically achieved by changing the orientation of the propulsion unit or by using additional mechanisms responsible for directing the water jet. These solutions are characterized by high energy efficiency, high maximum thrust, and low operating costs. Due to the separation of thrust generation and steering functions, dynamic maneuvering at high speeds is possible without a significant loss of power.

A classic example of such control is a system consisting of a propeller and a rudder [12]; however, in many modern designs, steering is performed by rotating the entire propulsion unit. Such a solution is used, for example, in the Protector military boat (Fig. 2.1b), where the thrust direction is changed by rotating the engine column. Systems of this type are also easy to integrate with autonomous systems, which favors their wide use in existing floating structures [6].

The second common type of design is a system with two independent propellers, placed at a certain distance from each other, which eliminates the need for a rudder. This solution is characterized by a simple mechanical structure, lacking moving parts other than the motor rotors, and great ease of control. Maneuvering is performed differentially by varying the thrust on opposite sides of the center of hydrodynamic resistance. The difference in generated forces creates a torque that induces rotation of the unit about the vertical axis. A disadvantage of the dual-motor system is the need for two independent propulsion units, which increases construction costs, especially for larger vessels. In systems based on internal combustion engines, thrust control may be less efficient than in the case of electric systems. Limitations may also arise from the inability to increase thrust on one side, which forces its reduction on the opposite side and leads to a decrease in the total power available for the maneuver. Designs of this type are not suited for dynamic turns at high speeds; however, they perform very well in applications requiring precise maneuvering at low speeds.

Due to their structural simplicity, ease of control, and high stability, dual-motor systems are commonly used in research units, especially catamarans. Thanks to the wide spacing of the hulls (pontoons), catamarans offer significant deck workspace, facilitating the integration of measurement equipment. Two motors allow for increased available power, although they may limit the maximum speed, making this type of design particularly useful in small, few-meter-long units used, among other things, for bathymetric surveys. Examples of such units include the WAM-V 2 platforms by Ocean Power Technologies (OPT) (Fig. 2.1a) and the FOKA research boat, built by the Solar Boat Team student research club at the Wrocław University of Science and Technology.

In addition to the two main categories, non-standard designs can also be distinguished, including all units that do not fit into the previously described groups. This category includes, among others, autonomous sailboats. These are powered exclusively by wind energy, and control is achieved by changing the position of the rudder or adjusting the sail's angle of attack, which affects the direction of the aerodynamic force acting on the sail. The advantage of such units is very high energy efficiency, resulting from the fact that the energy required for movement comes entirely from the wind. Despite this, autonomous sailing designs are not widely used due to their high dependence on weather conditions, the complexity of the control process, and the need for specific hull forms designed for sailing. An example of an autonomous sailing platform controlled by the sail's angle of attack are the units from Saildrone (Fig. 2.1c). Conversely, an example of an autonomous sailboat controlled by a classic rudder is the Passat (Fig. 2.1d), developed by the Konar student research club at the Wrocław University of Science and Technology.

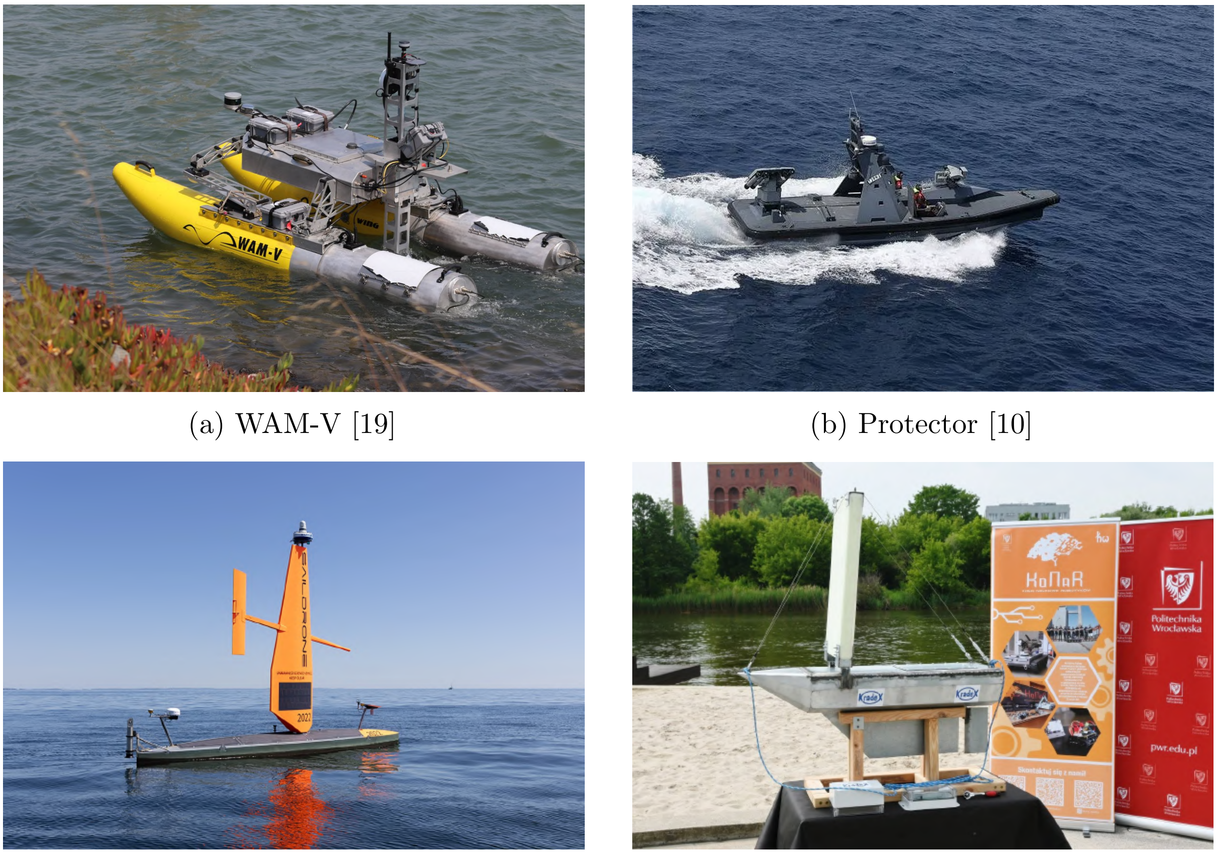

(a) WAM-V [19]

(b) Protector [10]

(c) Saildrone [22]

(d) Passat [14]

2.1 The "FOKA" Robot

The "FOKA" robot was developed for educational and research purposes by the "Project FOKA" team, operating within the "PWr Solar Boat Team" student research club at the Wrocław University of Science and Technology. This unit served as the testing platform for the selected control algorithms described in this thesis.

The robot's design is based on a catamaran-type hull consisting of two pontoons manufactured using the lamination method. Each pontoon measures 100 cm in length, 20 cm in width, and 15 cm in height, with a 30 cm spacing between the hulls. The total mass of the boat, including the research equipment, is approximately 15 kg. The pontoons are connected by aluminum profiles, which support a waterproof box containing the control electronics and the electrical system. The power source is a lithium-ion battery with a resultant 5S8P configuration (21 V, 21 Ah), constructed from four modules connected in parallel (Photo 2.3f), each having an internal 5S2P structure.

The differential steering system is implemented through a pair of ApisQueen U5 brushless motors [4] (Photo 2.3a) along with dedicated 2-6S 100 A Feather ESCs (Electronic Speed Controllers) [3] (Photo 2.3b) supporting PWM signals. This propulsion setup allows for independent control of the thrust generated by each motor. The vessel is equipped with a set of sensors necessary for the implementation and testing of autonomous control algorithms. The measurement system includes a Waveshare L76K GPS receiver [24] (Photo 2.3d), communicating with the onboard computer via a UART interface in the NMEA standard, and an Adafruit LSM9DS1 9DoF Inertial Measurement Unit (IMU) [16] (Photo 2.3c). The inertial module includes a triaxial accelerometer, gyroscope, and magnetometer, and communicates via the I^2C interface.

The onboard computer responsible for processing sensor data and executing control algorithms is a Raspberry Pi 4B platform (4 GB RAM) [1] (Photo 2.3e) running the Ubuntu 22.04 operating system. The ROS 2 Humble framework [20] is deployed on the computer to facilitate the integration of measurement modules, communication, and the execution of the vessel's motion control algorithms.

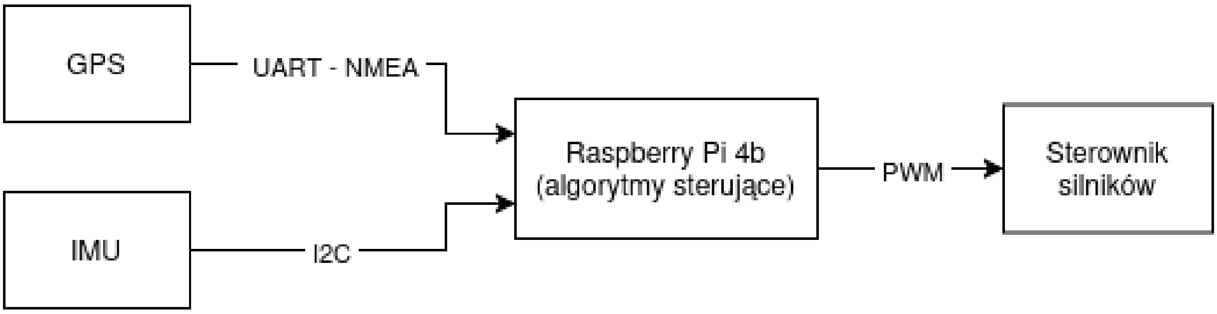

Figure 2.2: Information flow diagram of the FOKA boat.

Due to the possibility of physical testing using the available "FOKA" robot, the subsequent parts of this work consider its kinematic model and the control and navigation algorithms suitable for implementation on a differentially steered USV platform.

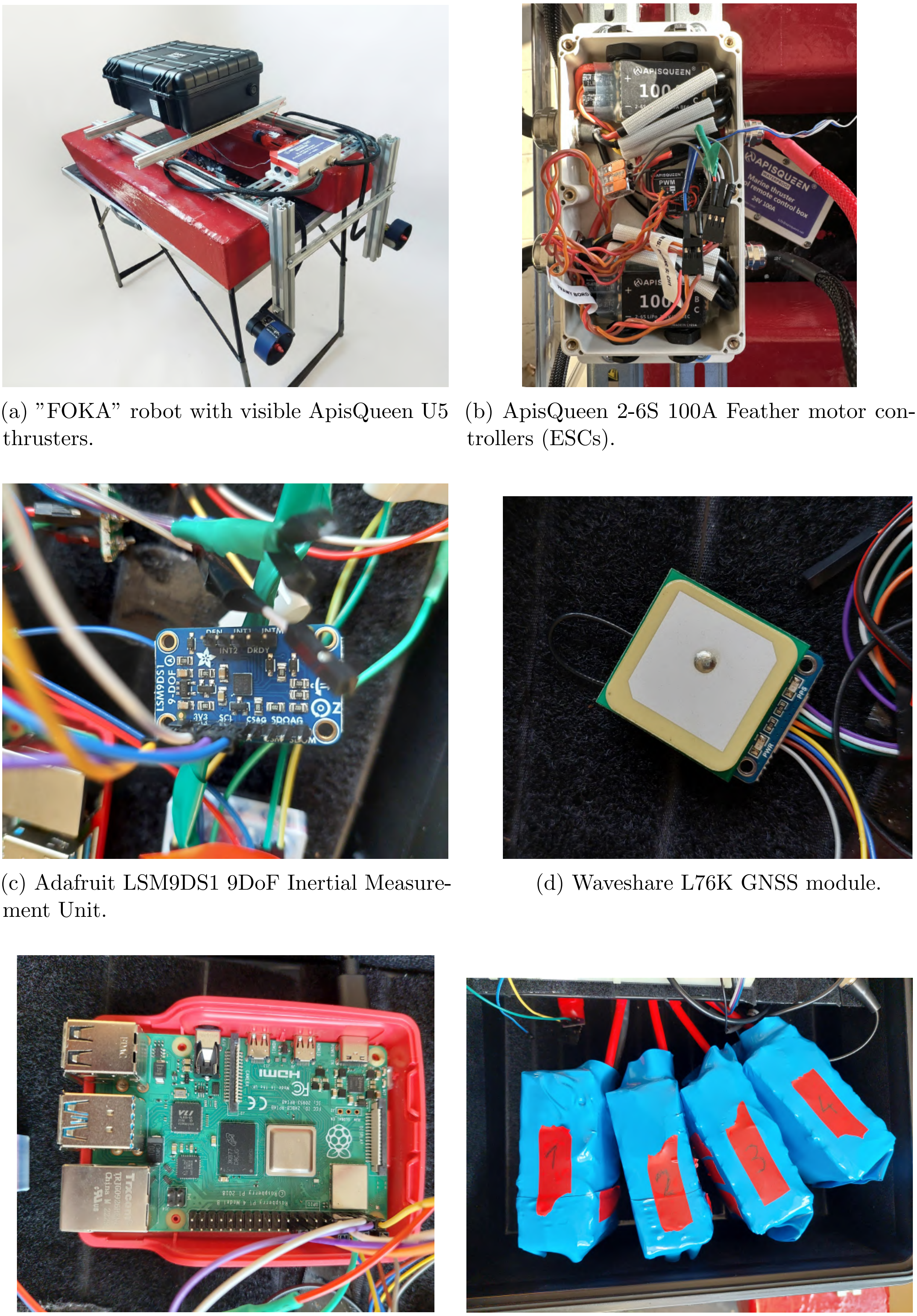

(a) ”FOKA” robot with visible ApisQueen U5 thrusters.

(b) ApisQueen 2-6S 100A Feather motor controllers (ESCs).

(c) Adafruit LSM9DS1 9DoF Inertial Measurement Unit.

(d) Waveshare L76K GNSS module.

(e) Raspberry Pi 4B platform.

(f) Li-ion batteries.

Figure 2.3: Selected photographs showing the construction and components of the ”FOKA” robot.

Chapter 3

Control Model

An object moving in an aquatic environment is treated as a rigid body in three-dimensional space, possessing six degrees of freedom (6 DOF). In accordance with maritime convention, translational motions along the axes of the body-fixed frame are defined as: surge (x), sway (y), and heave (z). The corresponding rotational motions are: roll (ϕ), pitch (θ), and yaw (ψ). Both translational and rotational motions are illustrated in diagram 3.1.

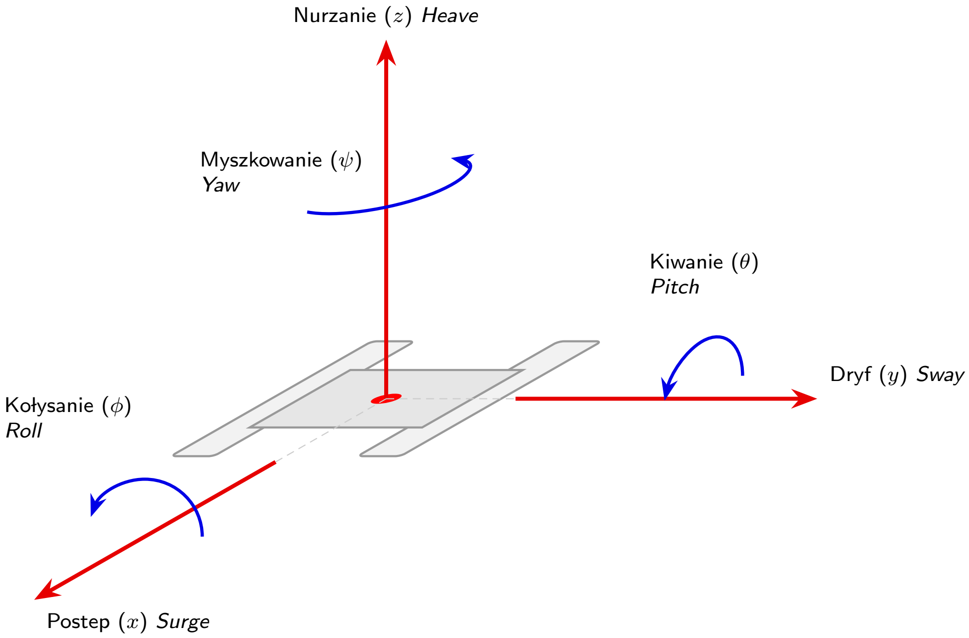
Nurzanie (z) *Heave*
Myszkowanie (ψ) *Yaw*
Kiwanie (θ) *Pitch*
Dryf (y) *Sway*
Kołysanie (ϕ) *Roll*
Postep (x) *Surge*

Figure 3.1: Diagram representing the 6 degrees of freedom of a USV in an aquatic environment.

In the analysis of surface vessel motion, several simplifications are typically adopted. Buoyancy, by counterbalancing the force of gravity, allows for the neglect of motion along the vertical axis (heave) under static conditions. Furthermore, hull geometry determines the stability of orientation in two degrees of freedom. While lateral tilts (roll, ϕ) may be significant for slender monohull vessels, a twin-hull construction (catamaran) is characterized by high transverse and longitudinal stability. Due to the large distance between the centers of buoyancy of the pontoons and the significant length of the hull, it is possible to omit roll (ϕ) and pitch (θ) dynamics during the control system design process.

These assumptions allow for the reduction of the mathematical model to three degrees of freedom (3 DOF), simplifying the problem to planar motion analysis, which is schematically shown in Figure 3.2. The kinematics of the catamaran, including the FOKA unit, is described by a system of equations transforming velocities from the local (body-fixed) frame to the global (inertial) frame (3.1) [13]:

$$\begin{aligned} \dot{x} &= u\cos\psi - v\sin\psi \\ \dot{y} &= u\sin\psi + v\cos\psi \\ \dot{\psi} &= r \end{aligned} \tag{3.1}$$

$\dot{x}$ – component of linear velocity along the OX axis in the global frame,

$\dot{y}$ – component of linear velocity along the OY axis in the global frame,

ψ – denotes the azimuth (heading/orientation) in the global frame,

u – longitudinal velocity (surge) in the local body-fixed frame,

v – lateral velocity (sway) in the local body-fixed frame,

r – angular velocity (yaw) around the vertical axis.

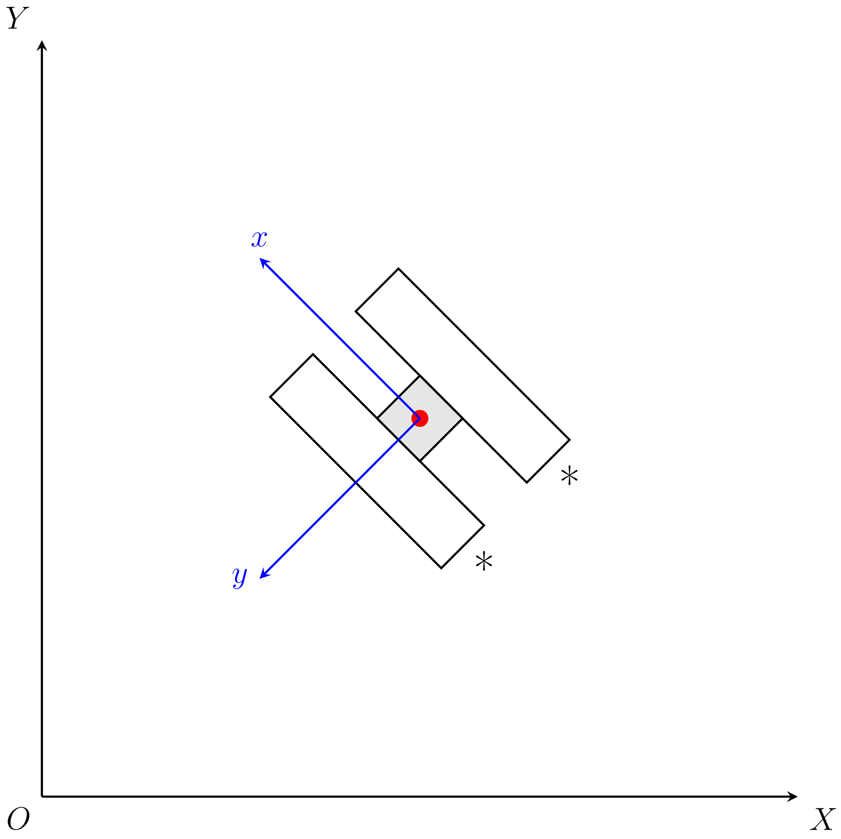

Figure 3.2: Diagram of coordinate systems: global (X, Y) and local USV (x, y). Stars indicate the locations of the motors at the stern of the vessel.

The dynamics of a surface vessel with three degrees of freedom (3-DOF) in the horizontal plane is described by the nonlinear vector equation (3.2) [13]:

$$M\dot{\nu} + C(\nu)\nu + D(\nu)\nu|\nu| = \tau \tag{3.2}$$

where:

M – denotes the inertia matrix (including rigid body mass and added mass),

$C(\nu)$– is the Coriolis and centripetal matrix,

$D(\nu)$– represents the hydrodynamic damping matrix,

ν – is defined as the vector of linear and angular velocities in the body-fixed frame.

The symbol τ denotes the vector of forces and moments generated by the motors.

Assuming hull symmetry relative to the longitudinal plane (typical for most vessels), the system matrices take the form presented in the system of equations (3.3):

$$
\begin{aligned}
M &= \begin{bmatrix} m_{11} & 0 & 0 \\ 0 & m_{22} & 0 \\ 0 & 0 & m_{33} \end{bmatrix} = \begin{bmatrix} m - X_{\dot{u}} & 0 & 0 \\ 0 & m - Y_{\dot{v}} & 0 \\ 0 & 0 & I - N_{\dot{r}} \end{bmatrix} \\
C(\nu) &= \begin{bmatrix} 0 & 0 & -m_{22}v \\ 0 & 0 & m_{11}u \\ m_{22}v & -m_{11}u & 0 \end{bmatrix} \\
D(\nu) &= \begin{bmatrix} d_{11} & 0 & 0 \\ 0 & d_{22} & 0 \\ 0 & 0 & d_{33} \end{bmatrix} = \begin{bmatrix} X_{u|u|} & 0 & 0 \\ 0 & Y_{v|v|} & 0 \\ 0 & 0 & N_{r|r|} \end{bmatrix} \\
\tau &= \begin{bmatrix} \tau_1 \\ \tau_2 \\ \tau_3 \end{bmatrix}
\end{aligned}
\tag{3.3}
$$

The parameters $X_{\dot{u}}$, $Y_{\dot{v}}$, and $N_{\dot{r}}$ are the so-called added mass coefficients. The physical interpretation of this phenomenon is related to the necessity for the hull to accelerate the surrounding mass of water, which results in an increase in the effective inertia of the system in the dynamic model. These values are strictly dependent on the hull geometry and are usually determined experimentally.

In turn, the coefficients $X_{u|u|}$, $Y_{v|v|}$, and $N_{r|r|}$ describe non-linear hydrodynamic damping. These forces, resulting from skin friction and form drag, approximately exhibit quadratic characteristics relative to velocity [17]. Similar to the added mass, these parameters require identification for the specific vessel design.

The control input vector, defining the impact of the propulsion system on the vessel's dynamics, takes the form $\tau = [\tau_1, \tau_2, \tau_3]^T$. The component τ_1 represents the resultant thrust force acting along the longitudinal axis of the hull, while τ_3 constitutes the rotational moment around the vertical axis, resulting from the asymmetry of thrusts generated by the thrusters (differential steering).

In the case of a standard catamaran design not equipped with transverse thrusters (so-called bow thrusters), the system is classified as *underactuated*. This means there is no possibility of directly generating force in the transverse axis, which is formally expressed by the condition $\tau_2 = 0$. It should also be noted that in a differential drive configuration, the components τ_1 and τ_3 are strictly coupled and depend on the geometric arrangement of the thrusters relative to the vessel's axis of symmetry.

Chapter 4

Control and Navigation Algorithms

In the classical sense, the control task is defined as determining the control input vector τ (which, in a differential configuration, is a function of the thrusters' thrust) that guarantees the achievement of the specified kinematic and dynamic parameters of the object. For Unmanned Surface Vehicles (USVs), open-loop control is insufficient due to the harsh nature of the environment and the presence of significant external disturbances, which lead to the accumulation of errors over time. Therefore, it is essential to close the control loop through a navigation system that provides real-time feedback (state estimation) for all controlled degrees of freedom.

4.1 Classical Navigation

Classical navigation is based on measurements performed relative to external reference frames. The primary quantities used in this approach are: the ship's position determined relative to the global coordinate system (e.g., based on GPS readings or sextant measurements) and the vessel's orientation expressed as a compass heading, determined using a compass, a mariner's compass, or observations of celestial bodies. In electronic systems, GNSS (Global Navigation Satellite Systems) and magnetometers serve as the primary sources of this data, enabling the measurement of the Earth's magnetic field vector.

This type of navigation has been used since the creation of the first watercraft. Its natural character stems from the fact that the simplest observations of position and direction can be made visually relative to the coastline. A breakthrough in the development of navigation methods was the discovery of the magnetic needle, used in China as early as the 11th century and becoming widespread in Europe from the 13th century. Another key invention was the chronometer designed in 1761 by John Harrison, which allowed for the precise determination of longitude. This solution was developed in response to a competition announced in 1714 by the British government, the goal of which was to devise a method for accurately determining longitude at sea. Precise timekeeping made it possible to calculate both latitude (following principles known for centuries through measurements of the altitude of celestial bodies) and longitude—by comparing local time with the time at a reference point of known location. Combined with the compass, these inventions made navigation possible from any point on Earth.

In classical navigation, determining the azimuth (bearing) leading to the target is crucial—this is the compass heading that must be maintained to travel from point $W_1(\phi_1, \lambda_1)$ to point $W_2(\phi_2, \lambda_2)$. For this purpose, the formula for the angle between two points on the surface of a sphere is used, as given in Equation 4.1. For long-distance navigation, the azimuth may require additional tabular corrections to account for the influence of wind and sea currents; however, this is not necessary in the case considered here.

ϕ_1 - latitude of the starting point (positive for the Northern Hemisphere, negative for the Southern).

ϕ_2 - latitude of the end point (positive for the Northern Hemisphere, negative for the Southern).

λ_1 - longitude of the starting point (positive for eastern longitudes, negative for western).

λ_2 - longitude of the end point (positive for eastern longitudes, negative for western).

$\Delta\phi$ - difference in latitude: $\Delta\phi = \phi_2 - \phi_1$.

$\Delta\lambda$ - difference in longitude: $\Delta\lambda = \lambda_2 - \lambda_1$.

R - Earth's radius expressed in meters (6,378,137 m).

θ - azimuth (bearing) from the starting point to the end point, calculated according to the formula:

$$\theta = \operatorname{atan2}(\sin(\Delta\lambda)\cos\phi_2,\ \cos\phi_1\sin\phi_2 - \sin\phi_1\cos\phi_2\cos(\Delta\lambda)) \tag{4.1}$$

During navigation, it is equally important to determine the distance between the vessel's current position $W_1(\phi_1, \lambda_1)$ and the target position $W_2(\phi_2, \lambda_2)$. The Haversine formula is used for this purpose, allowing for the calculation of distances between points on the surface of a sphere, according to Equation 4.2.

$$\begin{aligned} a &= \sin^2\left(\frac{\Delta\phi}{2}\right) + \cos\phi_1\cos\phi_2\,\sin^2\left(\frac{\Delta\lambda}{2}\right), \\ d &= 2R\cdot\operatorname{atan2}\big(\sqrt{a},\ \sqrt{1-a}\big) \end{aligned} \tag{4.2}$$

To read the boat's current azimuth, a compass or a mariner's compass can be used. In electronic systems, this direction is determined based on magnetometer readings, which measure the direction of the Earth's magnetic field vector rather than the direct direction of geographic North. Therefore, one must account for magnetic declination (the constant difference between the magnetic and geographic poles, which is approximately 5° East for Wrocław) and deviation (error resulting from local electromagnetic interference). The compass azimuth can be calculated using the trigonometric function `atan2()`:

$$\begin{aligned} \theta &= \operatorname{atan2}(y, x), \\ \theta' &= \theta + d + \delta \end{aligned} \tag{4.3}$$

θ' - true azimuth (heading),

θ - azimuth read from the compass or magnetometer,

d - magnetic declination,

δ - magnetic deviation,

(y, x) - horizontal components of the magnetic field vector.

Classical navigation using GNSS systems is very effective over long distances and wherever high measurement precision is not required. However, it should be noted that civilian localization systems offer accuracy on the order of several meters, which is sometimes insufficient in inland waters such as rivers, or when performing precise bathymetric mapping or monitoring the chemical parameters of water bodies. In such situations, it is necessary to apply more advanced localization methods or measurement filtration.

4.2 Dead Reckoning Navigation

Dead reckoning (DR) consists of determining the current position based on displacement and orientation measurements in the vessel's body-fixed reference frame, and then converting them into global coordinates. Due to its independence from external measurements, it was one of the primary navigational methods used in conditions that made astronomical observations impossible—for example, during heavy cloud cover or before the development of precise methods for determining longitude.

An example of the effectiveness of dead reckoning is the feat of Frank Worsley during Ernest Shackleton's Antarctic expedition in 1916. For 17 days, he steered a small lifeboat over a distance of approximately 1,300 km, relying solely on estimations of heading, speed, leeway, and the impact of ocean currents. Verification of the calculations was only possible sporadically every few days when the sun briefly emerged above the horizon. Despite extreme conditions and the low stability of the vessel in the turbulent Scotia Sea, Worsley managed to lead the crew from Elephant Island to South Georgia, enabling the rescue of all expedition members. This story serves as an example of the surprising effectiveness of dead reckoning methods, even with limited measurement accuracy.

Dead reckoning is fundamentally based on two parameters: heading and speed. Knowing these, it is possible to determine the vessel's velocity vector and then—through integration over time—calculate the displacement relative to the starting point. In traditional seafaring, the heading was determined using a mariner's compass or by observing points on the horizon, while the speed was measured using a chip log: a line with knots dropped from the stern of the ship. Based on the number of knots that emerged from the water within a specified time, the speed was determined in knots (1 kn = 1 nm/h). Over longer distances, corrections for wind, sea currents, and course deviations had to be additionally accounted for, though in calm sea conditions, their impact could be negligible.

In electronic systems, the roles of the log and compass are taken over by accelerometers and gyroscopes. These sensors provide measurements of linear accelerations and angular velocities, allowing for trajectory determination through double integration. Modern inertial measurement units (IMUs) enable high-frequency and high-resolution measurements. However, this method is burdened with a time-accumulating error resulting from the accumulation of measurement inaccuracies and noise. This phenomenon is known as sensor drift. For this reason, dead reckoning is rarely the sole method used to determine displacement.

4.3 Hybrid Navigation

In applications where precise boat localization is required during relatively small displacements but over long-duration measurements, the most advantageous solution is the use of hybrid navigation. This method combines the advantages of dead reckoning with classical methods based on external reference systems, such as GPS or vision systems.

In the hybrid approach, the vessel's position is determined simultaneously based on measurements from the local system (including accelerometers, gyroscopes, or encoders) and data relating to the global system. Combining these two information sources allows for the mitigation of the typical errors of both methods—the drift characteristic of dead reckoning and the low frequency, quality, or temporary unavailability of external measurements.

The process of combining information from multiple sensors to obtain a more accurate and noise-resistant estimate is called *sensor fusion*. Fusion methods, such as Kalman filters and their nonlinear extensions, are currently the standard in navigation systems used in mobile robotics.

The Kalman filter is a recursive algorithm that determines the estimate with the minimum error variance for a linear dynamic model. Its application in robotics is widespread due to its computational efficiency and its key role in sensory data fusion.

The algorithm's operation is based on a state-space model of the system, defined by two equations: the state evolution (transition) equation (4.4) and the observation (measurement) equation (4.5) [15]:

$$x_k = Ax_{k-1} + Bu_{k-1} + w_{k-1} \tag{4.4}$$

$$z_k = Hx_k + v_k \tag{4.5}$$

In equation (4.4), used in the prediction phase, A is the state transition matrix, B is the control matrix, and vector w represents the process noise (model inaccuracies, external disturbances). Equation (4.5) describes the relationship between the actual state and the measurement z_k through the observation matrix H. Vector v models the measurement noise resulting from sensor imperfections. The filter's duty cycle consists of alternating phases of prediction (based on the model) and correction (based on the measurement z_k).

The classical Kalman filter assumes the linearity of the dynamics model (constant matrices A and H). Due to the nonlinear characteristics of the described USV unit (Equation 3.2), resulting mainly from quadratic hydrodynamic damping, the direct use of a linear algorithm would lead to erroneous estimation. Therefore, in the practical implementation of the system (Chapter 6), an Extended Kalman Filter (EKF) was used. This algorithm linearizes the object's model at the current operating point, which allows for effective state estimation despite the system's nonlinearity.

4.4 Implementation of Differential Steering

Boat control is implemented using two control variables: a steering parameter $d \in [-1, 1]$, acting as a steering wheel, and a velocity parameter $v \in [-1, 1]$, acting as a throttle. The value of v determines the direction and maximum magnitude of the thrust generated by the motors, where $v = 1$ corresponds to maximum forward thrust, $v = 0$ signifies no thrust, and $v = -1$ defines maximum reverse thrust. Conversely, the parameter d is responsible for controlling the direction of motion through differential thrust distribution between the motors, where $d = 1$ represents a maximum right turn, $d = 0$ straight-ahead motion, and $d = -1$ a maximum left turn. This control scheme corresponds to a classical "throttle-steering" model, in which the magnitude v determines the longitudinal velocity, while the parameter d dictates the change in direction through thrust asymmetry.

The thrusts generated by the left (T_L) and right (T_R) motors are determined based on the following functions:

$$T_L(v,d), \quad T_R(v,d) \in [-1,1].$$

After calculation, these values are converted into the pulse width of the PWM signal controlling the motor controllers (ESCs). The transformation is defined by the following piecewise dependencies:

$$T_L(v,d)[\%] = \begin{cases} v \cdot 100\%, & \text{if } d \leq 0, \\ v(1-2d) \cdot 100\%, & \text{if } d > 0, \end{cases} \tag{4.6}$$

$$T_R(v,d)[\%] = \begin{cases} v(1+2d) \cdot 100\%, & \text{if } d \leq 0, \\ v \cdot 100\%, & \text{if } d > 0. \end{cases} \tag{4.7}$$

This method of determining motor thrust enables smooth differential steering, where parameter d limits the intensity of one of the motors depending on the turn direction, and parameter v determines the overall level of generated thrust. Although this solution reduces the total thrust of the boat, it protects it from an excessive increase in RPM and reduces its speed during maneuvers, where the risk of damage may be higher.

The final stage of the control chain is the conversion of the determined normalized thrust $T \in \{T_L, T_R\}$ into a control signal compatible with the Electronic Speed Controllers (ESC). This signal takes the form of a Pulse Width Modulation (PWM) signal. For a thrust value $T \in [-1,1]$, the pulse width u_{pwm} expressed in microseconds $[\mu s]$ is calculated according to the following relationship:

$$u_{pwm}(T) = 1500 + 450 \cdot T + 50 \cdot \operatorname{sgn}(T), \tag{4.8}$$

1500 – neutral value (motor at rest, $T = 0$),

450 – gain coefficient scaling the control range,

50 – constant compensating for the motors' deadband,

$\operatorname{sgn}(T)$ – signum function, returning the sign of the thrust value.

4.5 Point-to-Point Control

In classical point-to-point navigation algorithms, the key task is to determine the desired bearing, which allows the vessel to move from a starting point A to a target point B (4.1). For differentially driven Unmanned Surface Vehicles (USVs), heading control (ψ, yaw) is most commonly implemented in a closed feedback loop using a PID (Proportional-Integral-Derivative) algorithm (4.1).

In practical implementation, the full PID structure is often reduced due to the specific characteristics of the controlled object. Given the vessel's significant inertia and frequent step changes in the desired heading value, the integral term (I) is often omitted. Furthermore, in systems where state estimation is burdened with significant measurement noise (e.g., when relying solely on data from a GPS receiver), the use of the derivative term (D) can lead to undesirable amplification of disturbances. It is worth noting that hydrodynamic resistance, which increases proportionally to the square of the surge velocity, introduces natural damping to the system, performing a function analogous to the derivative term.

The advantage of this approach is that it does not require the identification of the boat's full dynamic model or its hydrodynamic coefficients. However, it should be emphasized that while this method—assuming a sufficient power reserve of the propulsion system—guarantees reaching the target, it does not ensure precise tracking of the desired trajectory. The impact of environmental disturbances, such as wind or water currents, causes drift, which consequently leads to an extension of the actual distance traveled by the vessel relative to the optimal route.

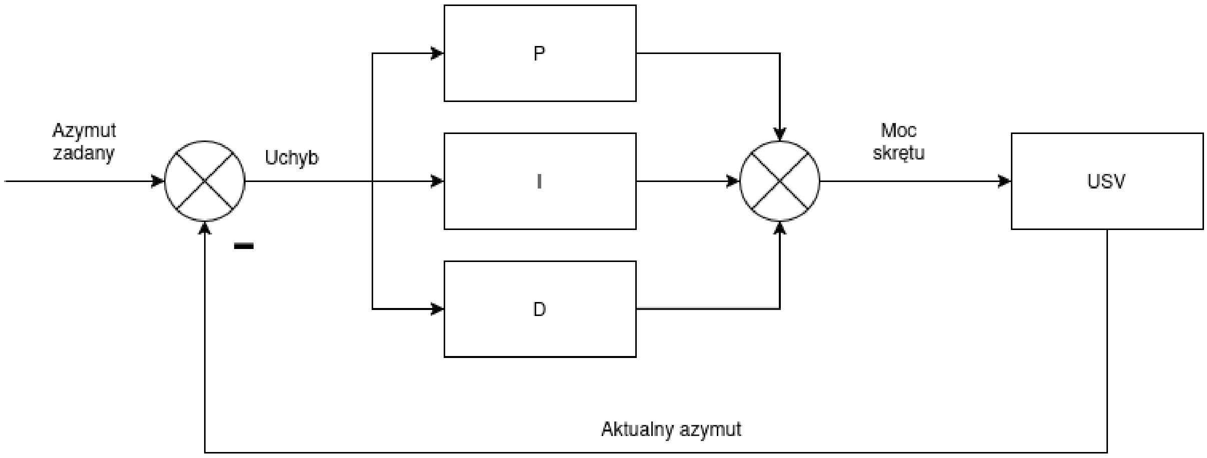

Figure 4.1: Diagram of the heading control system with feedback loop.

4.6 Trajectory Tracking – Compensation of Slow-Varying Disturbances

In simplified mathematical models of surface vessel dynamics, often only buoyancy, gravity, and the influence of the propulsion system are considered. In real-world operating conditions, however, the aquatic environment is characterized by the presence of significant external disturbances. The ship's hull is primarily affected by aerodynamic forces (wind) and hydrodynamic forces (currents, waves). In the context of path-following control, the resultant of these effects is usually modeled as a slowly varying disturbance with a constant direction and orientation in the global reference frame.

To ensure precise tracking of the desired trajectory, the control algorithm cannot be limited to merely determining the target bearing. It is necessary to introduce mechanisms to compensate for the drift phenomenon caused by the aforementioned environmental factors. One approach is the direct measurement of wind and current speed and direction, followed by their inclusion in the kinematic model. However, this method requires expensive and complex measurement equipment.

An alternative and more commonly used solution is to estimate the impact of disturbances based on the control error. This allows for effective drift compensation without the need to expand the sensor system. Algorithms that perform this task by applying an integral term in the control law include the ILOS (Integral Line-of-Sight) method [5] and the PID controller.

The trajectory tracking task for a USV is performed within a cascade control architecture. This structure assumes a hierarchical division of the system into two coupled control loops: the outer (navigation) loop and the inner (heading autopilot) loop. The task of the outer controller, based on the ILOS or PID algorithm, is to minimize the path error by determining the desired heading (ψ_d) for the sub-loop. The inner loop is responsible for stabilizing the vessel's orientation, directly controlling the actuators to achieve the desired angle (ψ). The dynamics of the inner loop must be significantly faster than the dynamics of the outer loop. In theoretical terms, this allows for the simplifying assumption that, from the perspective of the slowly-varying navigation loop, the inner loop is an object that responds instantaneously. The block diagram of the discussed cascade control structure for a USV is shown in Figure 4.2.

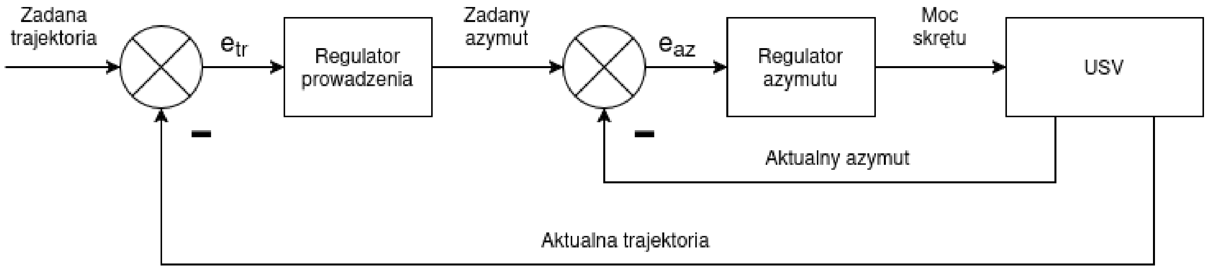

Figure 4.2: Block diagram of the USV cascade control system.

4.6.1 LOS and ILOS

The Line-of-Sight (LOS) control algorithm is a geometric guidance method that enables tracking of a desired trajectory by determining a setpoint heading angle [12]. In steady state, under ideal conditions, the vessel maintains a heading consistent with the path azimuth (Ψ_p). If a cross-track error occurs, the algorithm generates a correction by directing the vessel toward a virtual target point (p_{los}) located on the path. This point moves along the desired route in conjunction with the vessel's longitudinal motion. The key tuning parameter of the algorithm is the lookahead distance Δ, which determines the distance to the target point. In literature, it is assumed that the optimal value of Δ falls within the range of 2 to 5 ship hull lengths [5]. However, it should be noted that the classical LOS method does not guarantee the compensation of constant environmental disturbances (e.g., drift), which can lead to a steady-state error.

The formula for the desired heading angle (LOS control law) is expressed by the following equation (4.9):

$$\Psi_{los} = \Psi_p + \arctan\left(\frac{-y}{\Delta}\right) \tag{4.9}$$

Ψ_{los} – desired heading angle (target angle),

Ψ_p – path inclination angle (path azimuth),

y – cross-track error (perpendicular distance from the path),

Δ – lookahead distance.

The Integral Line-of-Sight (ILOS) control algorithm is an extension of the classical geometric LOS method, incorporating an additional integral term. The introduction of this element aims to compensate for the influence of constant environmental disturbances, which lead to steady-state errors in the standard system. By accumulating the cross-track

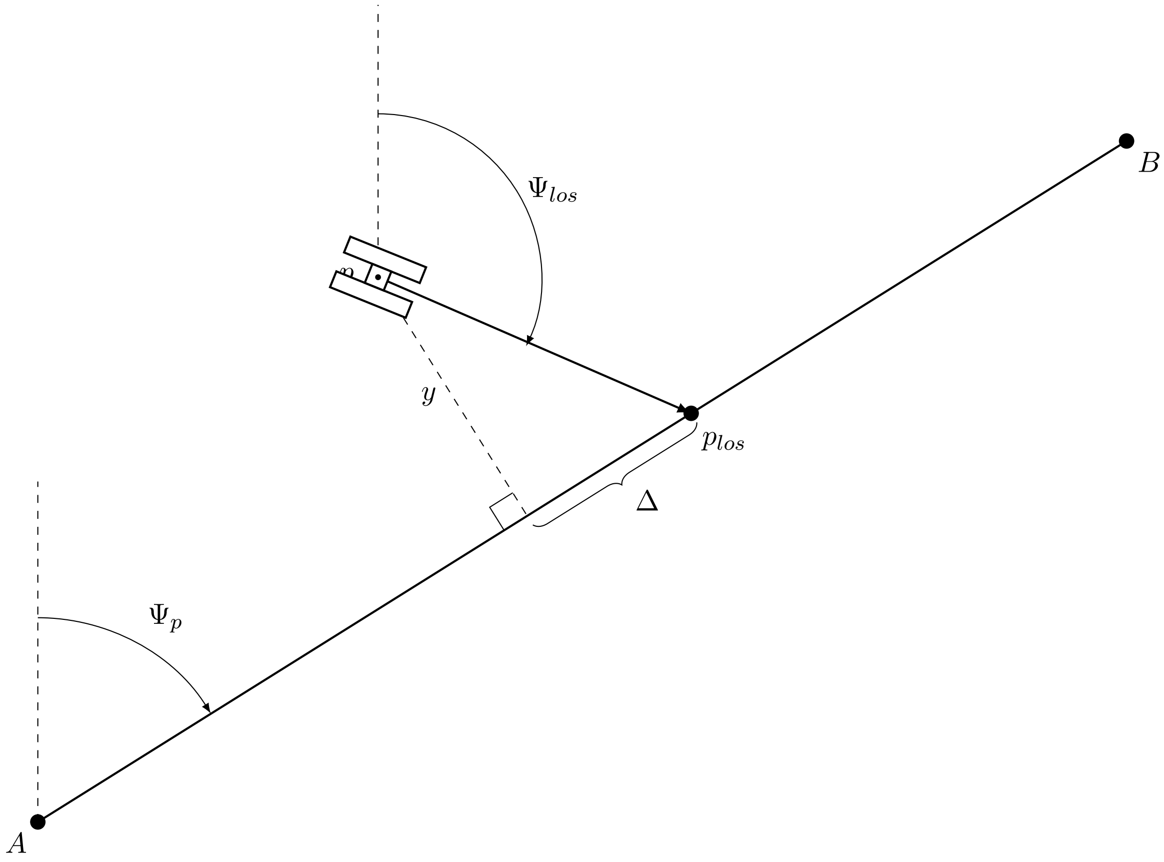

Figure 4.3: Principle of LOS operation.

error over time, the algorithm appropriately corrects the desired heading, eliminating the deviation from the path.

The control law determining the desired heading angle in the ILOS method is described by dependency (**??**) [5]:

$$\Psi_{los} = \Psi_p + \arctan\left(\frac{-y - \sigma y_{\text{int}}}{\Delta}\right) \tag{4.10}$$

where $\sigma > 0$ constitutes the gain coefficient of the integral term y_{int}. The dynamics of the integral component's value change is defined by the differential equation (4.11):

$$\dot{y}_{\text{int}} = \frac{\Delta y}{(y + \sigma y_{\text{int}})^2 + \Delta^2} \tag{4.11}$$

The presented form of the integral component dynamics equation (4.11) plays a crucial stabilizing role. The presence of state variables in the denominator introduces nonlinear damping, which limits the rate of growth of y_{int} at large errors. This mechanism acts as a built-in safeguard against integrator saturation (the so-called anti-windup function), preventing excessive overshooting of the control signal.

Chapter 5

Analysis of Control Algorithm Performance

5.1 Simulation Environment

In order to conduct a comparative analysis and verify the effectiveness of the developed control algorithms, a dedicated virtual environment was prepared. Gazebo Sim version 8.9.0 was selected as the simulation platform. This decision was driven by the native compatibility of this environment with the ROS 2 system (Jazzy distribution) and the availability of dedicated communication interfaces, which significantly facilitated the integration of the control system.

The simulations were conducted using the Maritime Gazebo package [2], which constitutes a specialized extension of the simulator with aquatic environment physics. The experimental scenery is based on a digital model of the *Sydney International Regatta Centre* race track, located at the geographic coordinates: latitude 33.7229° S, longitude 150.6709° E.

Due to the lack of a hydrodynamic model for the FOKA robot in the Gazebo environment, the kinematically similar WAM-V (Wave Adaptive Modular Vessel) model, available in the Maritime Gazebo library, was used to verify the algorithms. It should be emphasized that the use of a surrogate model in the simulation serves to verify the structure and operational logic of the implemented control algorithms. Due to differences in mass and hydrodynamics between the simulated robot and the actual FOKA vessel, specific controller gain values (tuning) cannot be transferred directly; however, the tuning methodology and system architecture remain identical. Detailed physical and geometric parameters of the WAM-V boat are summarized in Table 5.1. The representation of the vessel's motion dynamics and hydrodynamic interactions in the simulator was implemented based on Fossen's equations of motion [11]. Figure 5.1 shows a screenshot from the simulation.

The test environment also accounts for the influence of external disturbances. A free-surface wave model was implemented, though parameters generating waves with minimal amplitude were chosen. Additionally, to verify the system's robustness against wind forces, the `gz-sim-wind-effects-system` plugin was utilized. In the test scenario, a wind vector of 3 units was defined, directed along the global OX axis, with a force scaling factor of 0.2.

The logic layer of the control system was implemented in Python 3. To ensure transparency and reproducibility of the research, the complete source code of the simulation software has been made available in a public GitHub repository [21].

Parametr	**Symbol/Jednostka**	**Wartość**
Parametry inercyjne i geometryczne		
Masa kadłuba (baza)	m [kg]	180.0
Masa silnika (pojedynczy)	m_{eng} [kg]	15.0
Długość pływaka	L [m]	4.9
Moment bezwładności osi x	I_{xx} [kg·m^2]	120.0
Moment bezwładności osi y	I_{yy} [kg·m^2]	393.0
Moment bezwładności osi z	I_{zz} [kg·m^2]	446.0
Parametry hydrodynamiczne (tłumienie)		
Opór liniowy wzdłużny (surge)	X_u	-51.3
Opór kwadratowy wzdłużny	$X_{\|u\|u}$	-72.4
Opór liniowy poprzeczny (sway)	Y_v	-40.0
Opór liniowy pionowy (heave)	Z_w	-500.0
Opór obrotowy (roll)	K_p	-50.0
Opór obrotowy (pitch)	M_q	-50.0
Opór obrotowy (yaw)	N_r	-400.0
Układ napedowy		
Współczynnik ciagu	T_{coeff}	0.004422
Średnica śruby	D [m]	0.2
Gestość medium (woda)	ρ [kg/m^3]	1000
Sensoryka		
Czestotliwość IMU	f_{imu} [Hz]	50
Czestotliwość magnetometru	f_{mag} [Hz]	50
Czestotliwość GPS	f_{gps} [Hz]	10
Szum GPS (poziomy, std)	σ_h	1.7×10^{-5}
Szum GPS (pionowy, std)	σ_v	2.0×10^{-5}
Warunki poczatkowe symulacji		
Pozycja startowa x	x_0 [m]	-532
Pozycja startowa y	y_0 [m]	162
Orientacja startowa (yaw)	ψ_0 [rad]	1.0

Table 5.1: Zestawienie parametrów symulacyjnego modelu USV WAM-V

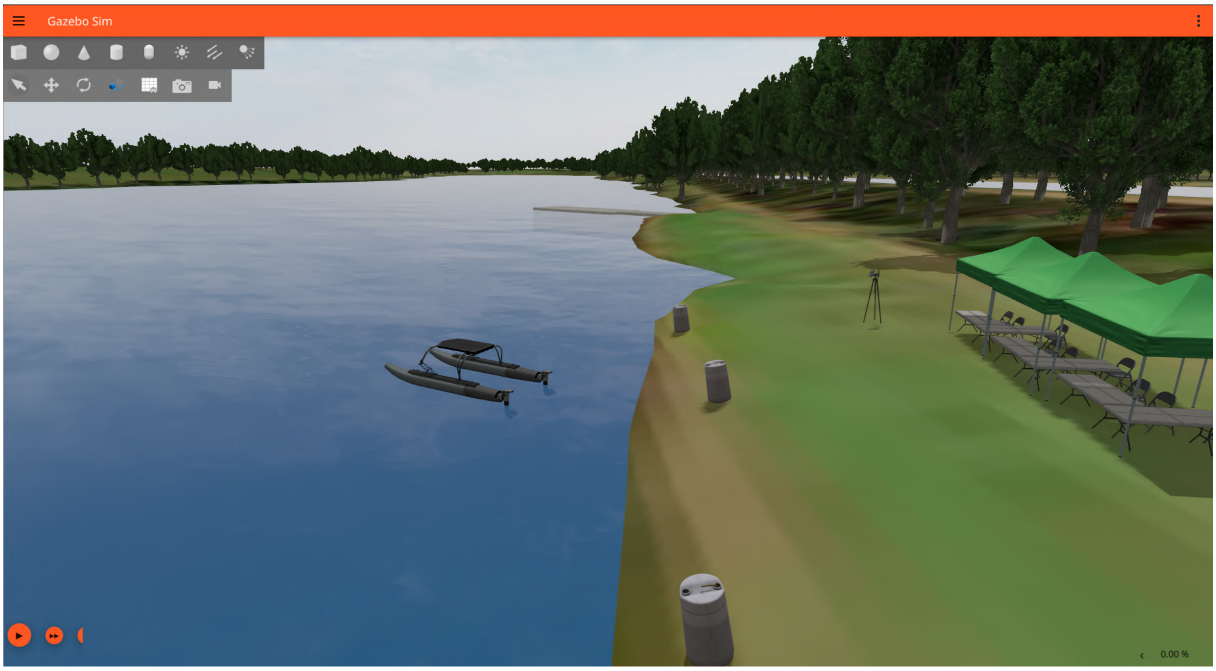

Figure 5.1: Screenshot from the Gazebo Sim simulation depicting the WAM-V boat at the Sydney International Regatta Centre.

5.2 Selection of Heading Controller Gains

Based on an analysis of relevant literature [26], it was assumed that the typical heading deviation of USV-class vessels from the setpoint under nominal operating conditions does not exceed 10°. However, considering the experimental nature of the "FOKA" platform and the specifics of projects within a student research club, it was decided to adopt a twofold safety margin. Consequently, the maximum expected heading error under normal conditions was defined as 20°.

To ensure control smoothness and protect the propulsion system, the selection of the proportional gain K_p was conducted while considering the physical constraints of the thrusters. A key design criterion was to prevent reverse operation of the motors (generating reverse thrust) at the maximum assumed error ($e = 20°$). This limitation aims to minimize the risk of cavitation at large heading angles, which could lead to nonlinearities in hydrodynamic characteristics and a potential loss of control stability.

According to the implemented thrust mixing algorithm, the condition for no reversal is met when the absolute value of the control signal $|d|$ is less than 0.5. For the threshold error $e = 20°$, this allows for the calculation of the maximum permissible gain value:

$$K_p = \frac{d_{max}}{e_{max}} = \frac{0.5}{20} = 0.025 \tag{5.1}$$

The adopted value of $K_p = 0.025$ represents a compromise between system dynamics (the speed of returning to the desired heading) and energy efficiency, alongside the minimization of mechanical wear on the motors.

Figure 5.2 presents the time-series responses of the system to a step change in heading with an initial error of 20°. The boat's reaction and the course of the control variable d are shown for the selected optimal gain ($K_p = 0.025$) and for alternative values, resulting in maximum control signals of $d = 0.4$ (conservative control) and $d = 0.6$ (aggressive control with reversal), respectively.

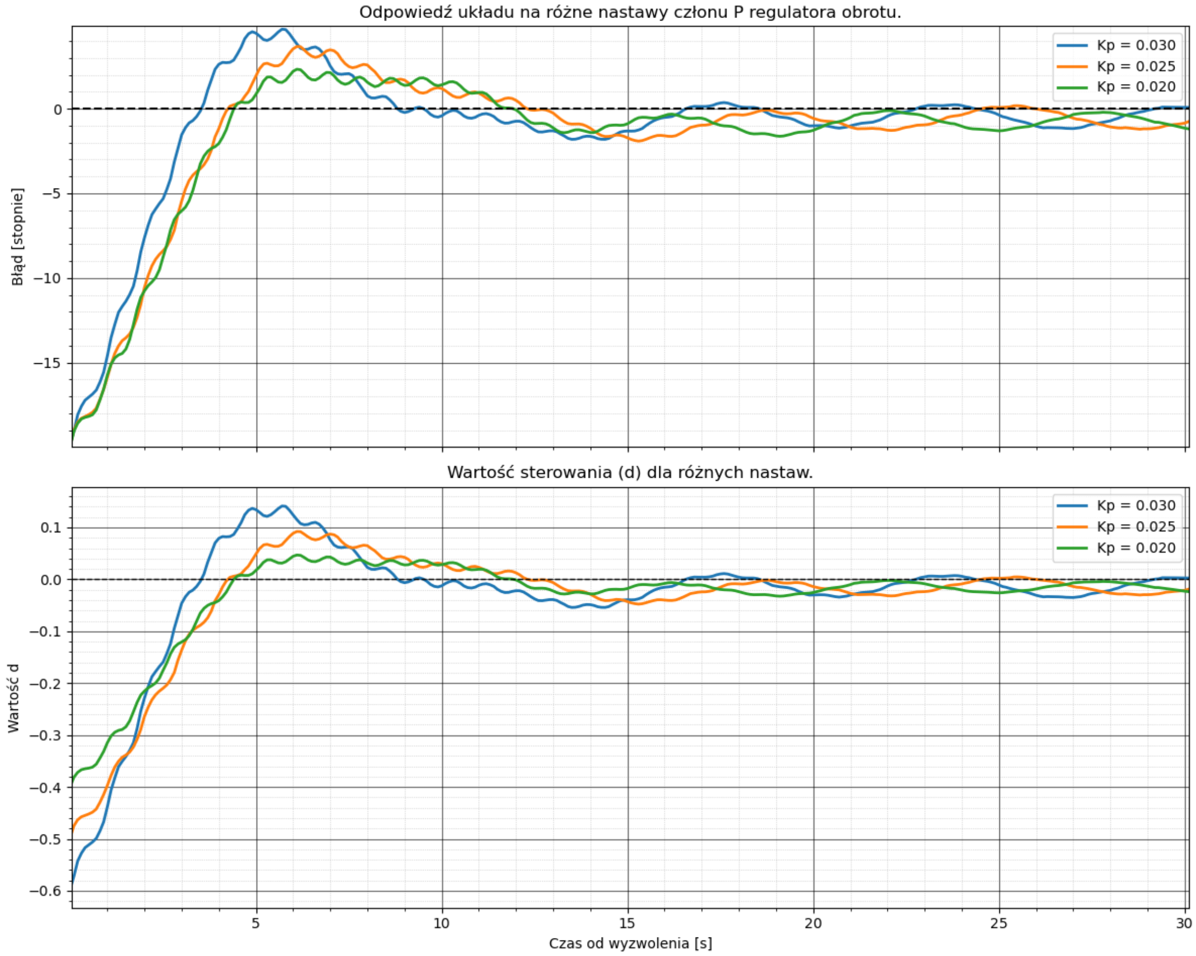

Figure 5.2: System response to different values of the proportional gain K_p of the heading controller.

To improve control quality and limit overshoot—which results from the adopted proportional gain—the heading controller structure was extended by adding a derivative term (D). The gain was selected through simulation experiments, using a compromise between oscillation damping and the system's operational speed as the primary criterion. The chosen value of $K_d = 0.5$ allowed for a twofold reduction in overshoot amplitude (decreasing from 4° to 2°). Crucially, the introduction of additional damping affected the system dynamics only slightly—the time to first reach the setpoint value increased by only 0.5 s (from 4.0 s to 4.5 s). The influence of the derivative term on the system's step response for various K_d values is presented in Figure 5.3.

5.3 Tuning of the ILOS Trajectory Controller Parameters

In order to determine the optimal values for the control algorithm parameters—specifically the lookahead distance Δ and the integral term gain σ—a series of simulation experiments was conducted. The test scenario involved following a straight-line trajectory defined by starting point $A(-33.72276; 150.67400)$ and end point $B(-33.72119; 150.67426)$. The total length of the test segment was 176.41 m. The simulation was initiated at zero initial

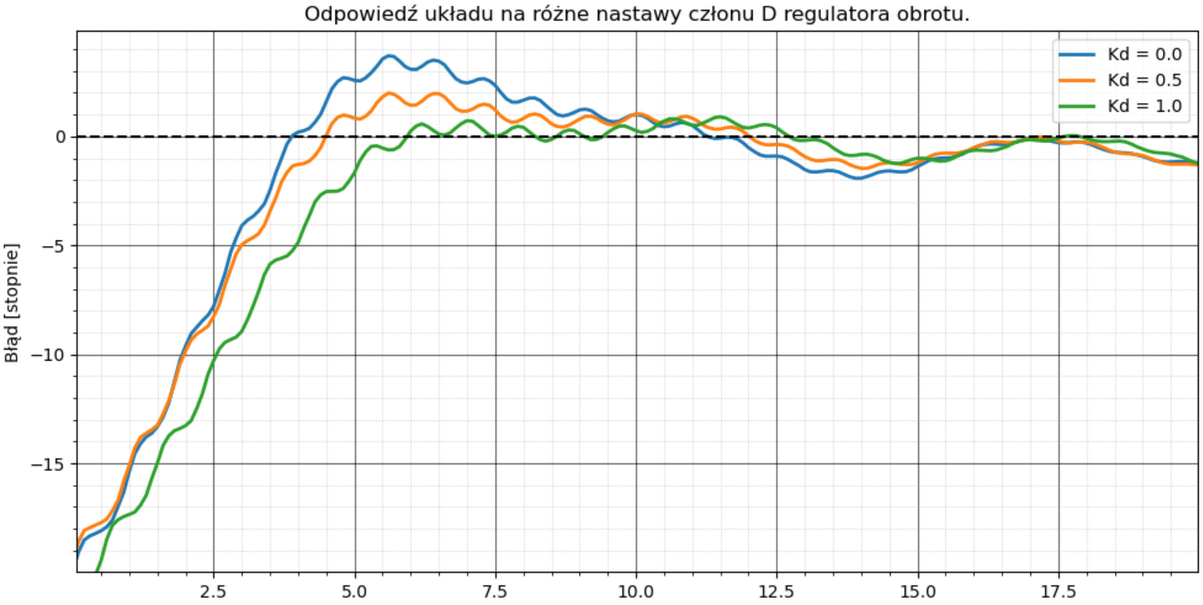

Figure 5.3: System response to different values of the derivative gain K_d of the heading controller.

velocity and with a heading error of 20° relative to the desired path azimuth.

According to the literature [8], the selection of parameter Δ is based on the rule that its value should not be less than twice the total hull length (L). This dependency directly affects the dynamics of the control system in a manner inversely proportional to the gain in a classical P-controller: higher Δ values result in a smoother approach to the path and smaller oscillations but increase the settling time. Lower Δ values provide a faster response but increase the risk of overshoot and instability.

Given the intended use of the "FOKA" research platform for operation in inland waters (rivers, lakes), the priority was to ensure relatively fast convergence to the desired trajectory, while accepting minor oscillations during the transient state. Through experimental testing, a value of $\Delta = 12.25$ m was selected, which corresponds to 2.5 times the hull length ($L = 4.9$ m). The chosen setting ensured that oscillations stabilized with an amplitude below 0.25 m after 20 s of simulation, which was considered a satisfactory result relative to the vessel's dimensions. The achieved settling time for the outer loop (20 s) is consistent with the operation time of the inner loop (heading autopilot), which has a settling time of approximately 4 s, thereby providing a fivefold safety margin.

In the first phase of tuning, to isolate the influence of the Δ parameter, the integral coefficient σ was set to zero, reducing the ILOS algorithm to the classical LOS version. As a result, a steady-state error of approximately -2.4 m was observed (for the chosen Δ value). The system response curves for various values of parameter Δ (with $\sigma = 0$) are presented in Figure 5.4.

The coefficient σ was determined experimentally by examining the system response for a fixed Δ and varying integral gain values. A value of $\sigma = 0.85$ was adopted as the optimal setting. The selection criteria included the first zero-crossing of the error before half of the simulation time had elapsed and limiting the oscillation amplitude to below 0.5 m. The responses for various σ values are presented in Figure 5.5.

Despite the tuning of the parameters, the system exhibits oscillations in the steady state. Reducing them by increasing the Δ parameter is not feasible due to the requirement for a short settling time. This indicates that, in the analyzed case, utilizing a classical PID controller might prove to be a more effective solution.

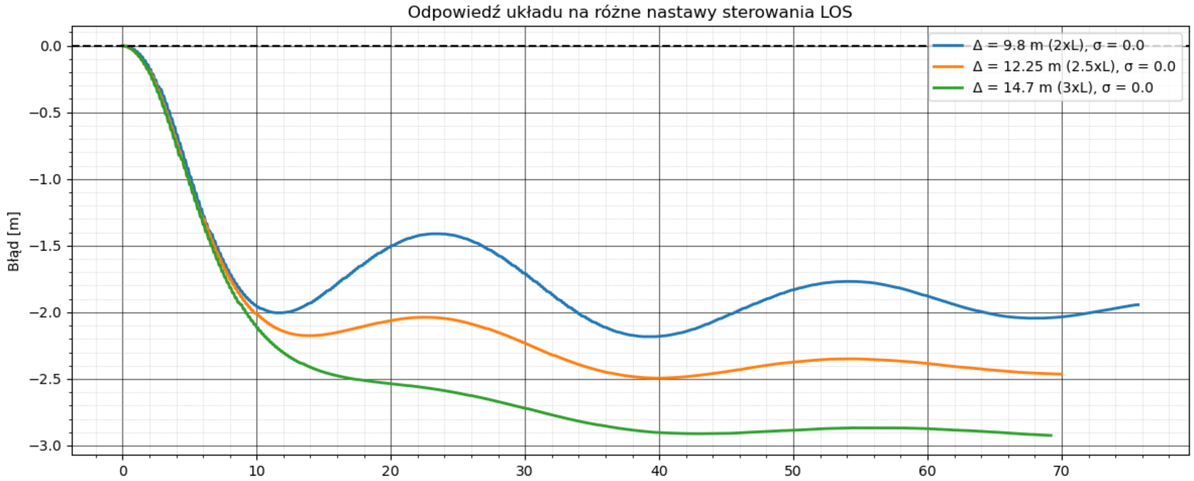

Figure 5.4: System response to various Δ parameter values with the integral term disabled.

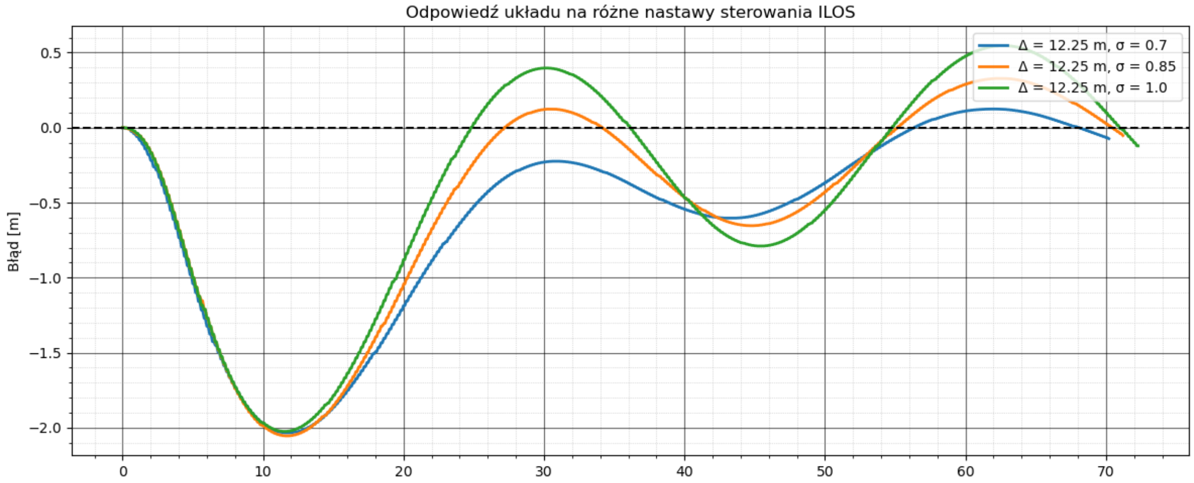

Figure 5.5: System response to various σ parameter values.

5.4 Tuning of the PID Trajectory Controller Parameters

To determine the PID trajectory controller gains, simulation tests were conducted in a scenario identical to that used for tuning the ILOS controller. The first stage involved finding the ultimate gain K_u of the proportional term. The value at which sustained oscillations occurred was found to be 9.5. Figure 5.6 illustrates these oscillations—their amplitude initially grows and subsequently stabilizes. The determined oscillation period T_u was 24 s.

For the initial selection of the K_i parameter, the Ziegler-Nichols method for a PI controller was employed. The calculated gains were $K_p = 4.275$ and $K_i = 0.214$. The system response for these settings (Figure 5.7) demonstrated stability; however, the initial oscillation amplitude was excessive (over 1.5 m), and the error reduction was too slow.

Due to the unsatisfactory results of the Ziegler-Nichols method, the final gains were selected experimentally. The proportional gain K_p was set to 9.0, which ensured a high reaction speed while maintaining stability. The K_i value was set to 0.856. This allowed for the elimination of steady-state error within the first oscillation, which is crucial for operating over short distances. The derivative gain K_d was set to 25, which limited the oscillation amplitude without losing the smoothness of the zero-crossing. The influence of various settings on the system response is shown in Figure 5.8.

In the analyzed scenario, the PID controller achieved better results than the ILOS algorithm, providing a shorter settling time and smaller oscillations. However, this does not imply that it is a superior solution under all conditions. The adopted settings may not perform well under varying wind conditions or different wind directions. The PID controller also features a derivative term whose gain can be directly adjusted, allowing for the application of aggressive and less universal settings, unlike the ILOS controller. A performance comparison of both controllers is shown in Figure 5.9. The USV trajectory with wind compensation using the PID controller and without wind compensation is shown in Figure 5.10.

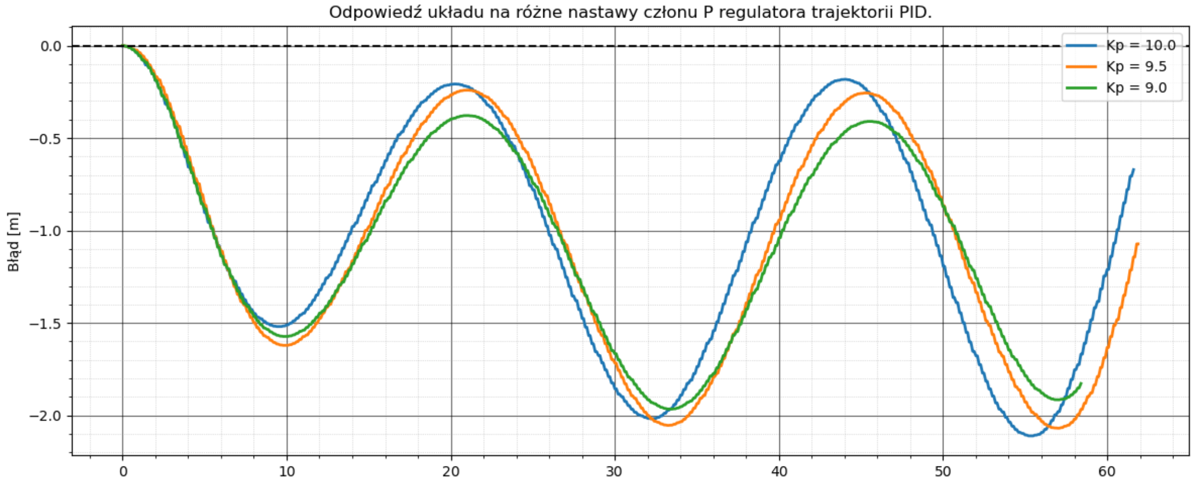

Figure 5.6: System response to various proportional gain K_p values for the PID trajectory controller.

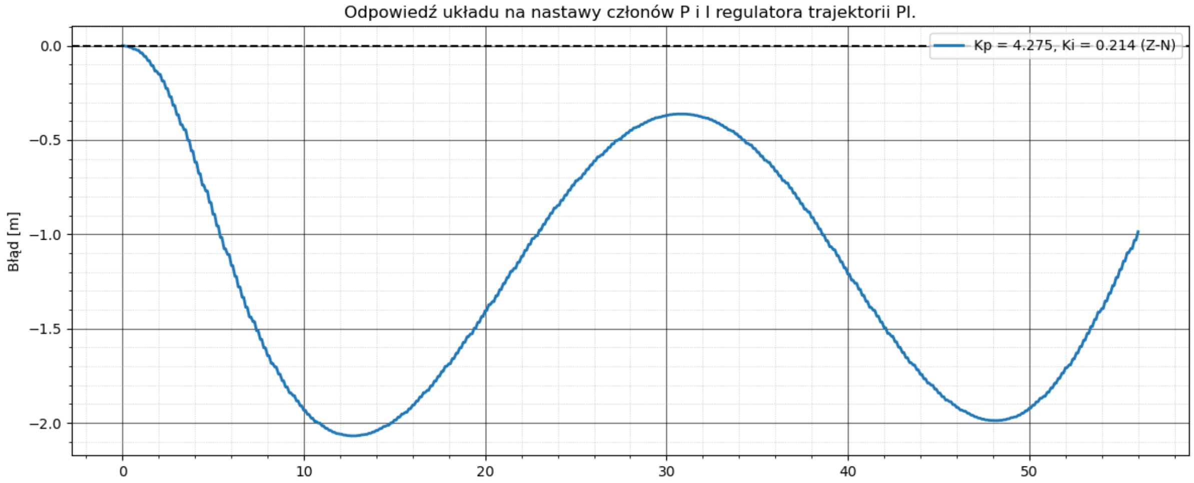

Figure 5.7: System response for K_p and K_i values calculated using the Ziegler-Nichols method.

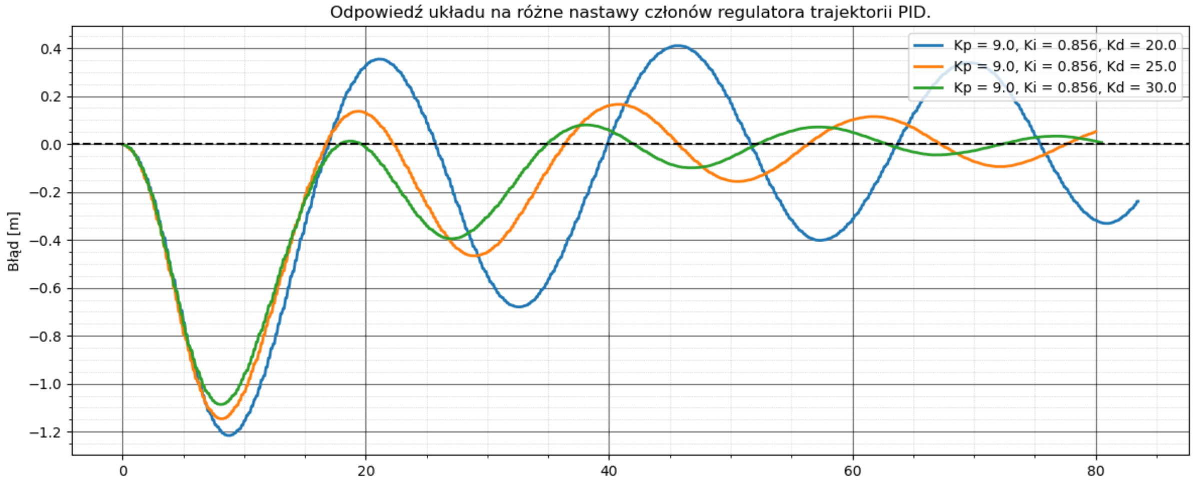

Figure 5.8: System response to various PID trajectory controller term values.

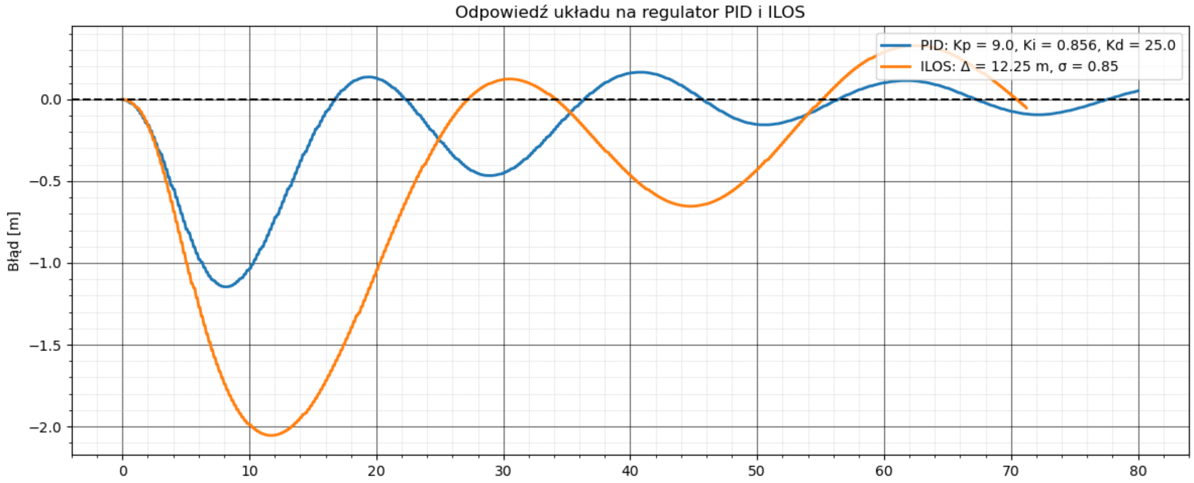

Figure 5.9: System response comparison between the PID and ILOS controllers.

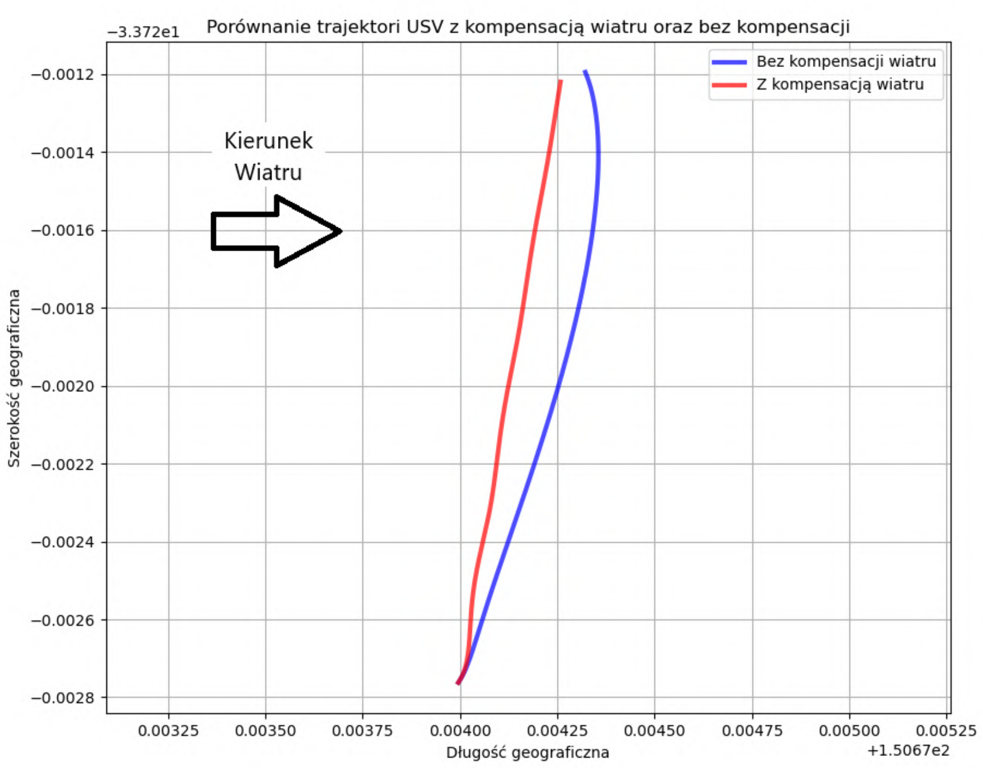

Figure 5.10: Comparison of trajectories with and without wind compensation.

Chapter 6

Comparative Analysis of Classical and Hybrid Navigation

6.1 Test Scenario

To conduct a comparative analysis of classical and hybrid navigation, a series of simulation tests was performed. The research scenario involved the movement of an Unmanned Surface Vehicle (USV) from a starting position W_0 (−33.722760; 150.674000) through a sequence of waypoints with coordinates W_1 (−33.721192; 150.674264), W_2 (−33.721365; 150.675368), and W_3 (−33.722538; 150.675245). The ultimate goal of the trajectory was a return to point W_1. The vehicle's guidance along the specified straight-line segments was implemented using an ILOS-type trajectory controller.

A key element of the simulation was the replication of the characteristics of a real Waveshare 76K GPS receiver. According to the device's technical specifications, the positioning accuracy, defined by the CEP (Circular Error Probable) parameter, is 2.0 m [25]. This value represents the radius of a circle within which the determined position is located with a 50% probability.

To implement this parameter in the state estimation algorithms, the CEP was converted into measurement noise variance. Assuming a normal distribution of errors, the standard deviation σ was determined according to relationship (6.1), using a conversion factor $\alpha \approx 0.849$:

$$\sigma = \alpha \cdot CEP \tag{6.1}$$

For the analyzed GPS module, the determined position variance (σ^2) was 2.88 m^2. Due to the imprecise nature of satellite measurements, the target point acceptance zone was defined as a circular area with a radius equal to the CEP error (2.0 m). This approach ensures that a waypoint is considered reached when the vessel's actual position coincides with the target, even in the presence of a large measurement error. A screenshot from Gazebo Sim showing the moment the WAM-V boat enters the acceptance zone marked by a marker is shown in Figure 6.2.

In the hybrid navigation variant, sensor fusion was applied using the ROS 2 `robot_localization` package [18], which implements the Extended Kalman Filter (EKF) algorithm.

The system architecture was based on the integration of data from an Inertial Measurement Unit (IMU) and a magnetometer, operating at a frequency of 50 Hz, with GPS position data provided at a frequency of 10 Hz. This allowed for the estimation of displacement and orientation in the local coordinate system while simultaneously correcting the global position.

In the absence of manufacturer data regarding the self-noise for the simulated sensor, the covariance matrix parameters were configured based on the TDK InvenSense ICM-20602 specifications. According to the technical documentation, the total RMS noise for the gyroscope is 0.04°/s, while for the accelerometer, this value is 1.0 mg. For the magnetometer, a standard deviation of 1.0 μT was assumed.

The architecture of the designed simulation system in the ROS 2 environment is based on data exchange between five independent nodes via topics, as shown in diagram 6.1. The central element of the structure is the `/ros_gz_bridge_node`, which functions as an interface performing bidirectional translation of messages between the Gazebo simulator's physics engine and the ROS standard. In the navigation layer, the `/navsat_transform_node` transforms raw GNSS data (`/gps/fix` topic) into the local coordinate system, feeding the `/ekf_filter_node`. This unit, which implements the Extended Kalman Filter, integrates position data with inertial measurements (`/imu`) and magnetometer data—pre-processed by the auxiliary `/CompassOdomNode`—to provide precise robot state estimation on the `/gps/filtered` topic. Based on the location determined in this way, the decision-making node `/Los_node` executes control algorithms, generating thruster control signals (`/right_thrust`, `/left_thrust`), which reach the simulation via the bridge. The applied modularity and hardware abstraction allow for the direct migration of the control software to the onboard computer of the target "FOKA" unit.

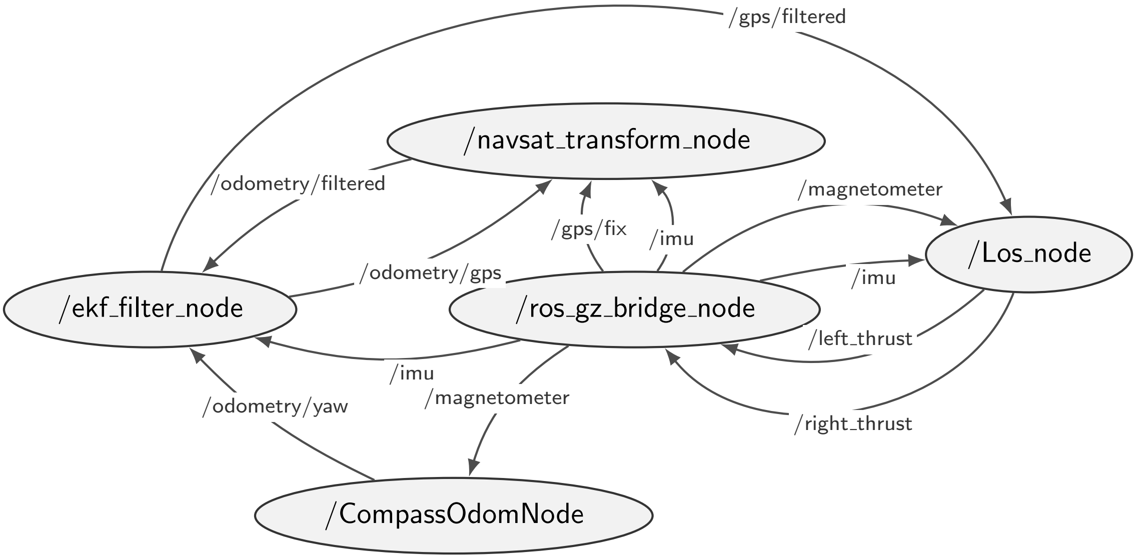

Figure 6.1: Graf przepływu danych w systemie ROS 2 (wizualizacja wezłów i tematów).

6.2 Results Analysis

Simulating the system's operation in the presence of measurement noise necessitated a modification of the internal heading controller (PD) settings. Due to the step-wise nature of changes in the estimated location and azimuth, the derivative term (D) introduced significant control errors that prevented stable trajectory tracking, resulting in the need to set its value to zero.

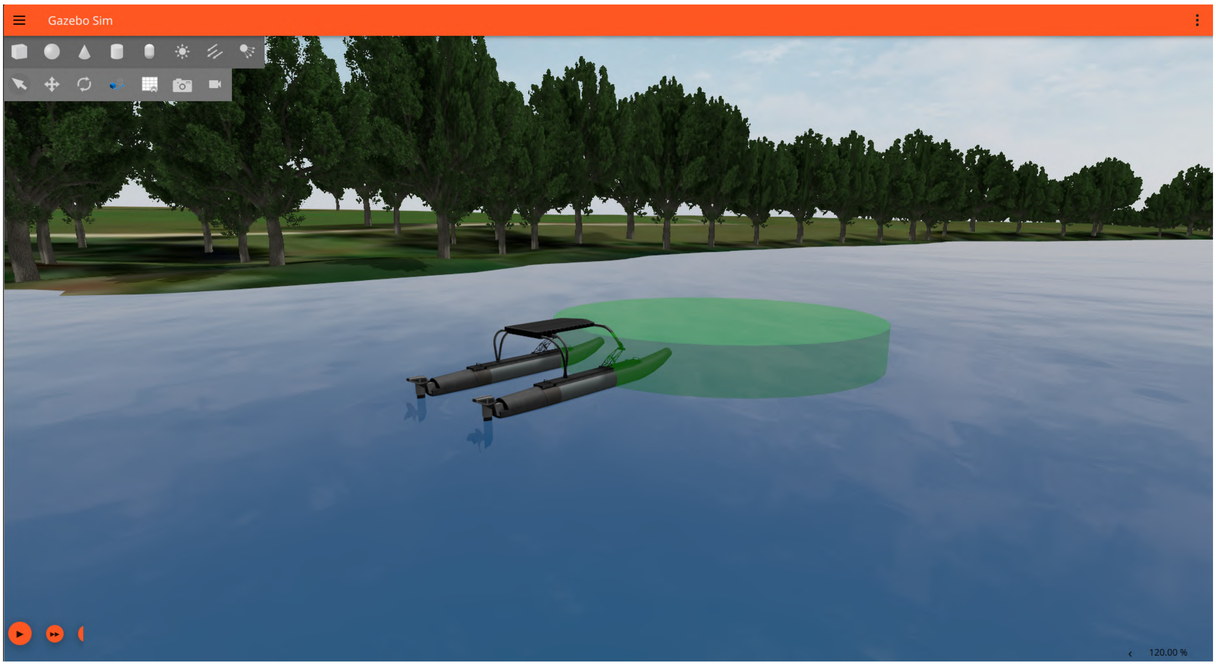

Figure 6.2: Screenshot from Gazebo Sim showing the moment the WAM-V boat enters the acceptance zone marked by a marker.

[Image of a PD controller block diagram]

The validation of the navigation algorithms was successful for both tested configurations. The USV unit reached all designated waypoints (W_0, W_1, W_2, and W_3) using both raw GPS data and sensor fusion. The actual trajectory of the vessel against the recorded measurement data is presented in Fig. 6.3 (raw GPS) and Fig. 6.4 (Kalman filter estimation). To visualize the distribution and characteristics of the measurement noise, enlarged fragments of the trajectory for raw and processed data are presented in Figs. 6.5a and 6.5b, respectively.

The comparative analysis reveals a significant advantage of the data fusion algorithm over the approach based solely on the GPS module. The application of an Extended Kalman Filter (EKF) combining satellite and inertial measurements allowed for an approximately 3.5-fold reduction in positioning error. The resulting Mean Absolute Error (MAE), oscillating around 40 cm, represents a performance that surpasses the typical accuracy of civilian GNSS receivers. A quantitative comparison of the positioning quality metrics is provided in Table 6.1, while the error time series for latitude and longitude are presented in Figs. 6.6b and 6.6a, respectively.

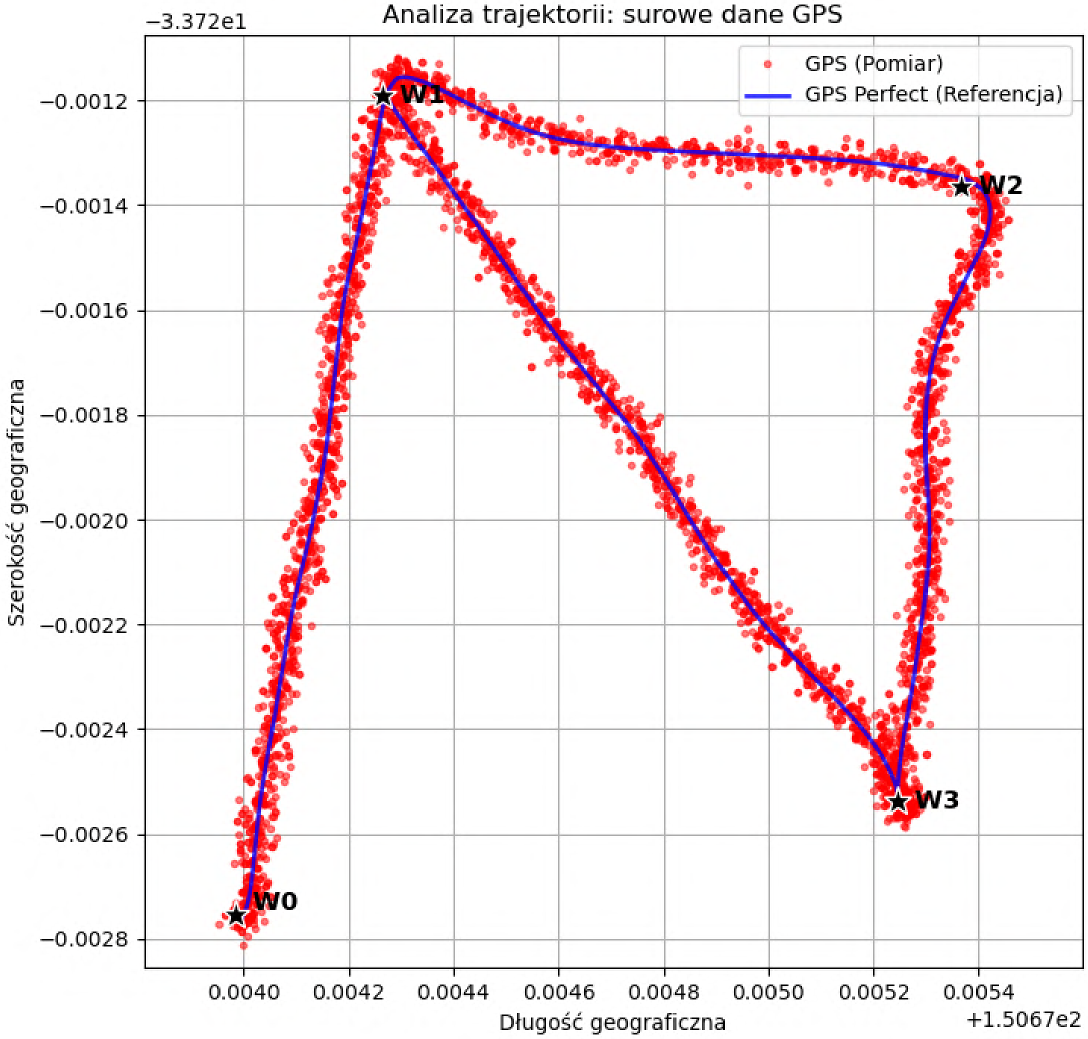

Figure 6.3: Trajectory with raw GPS measurement points.

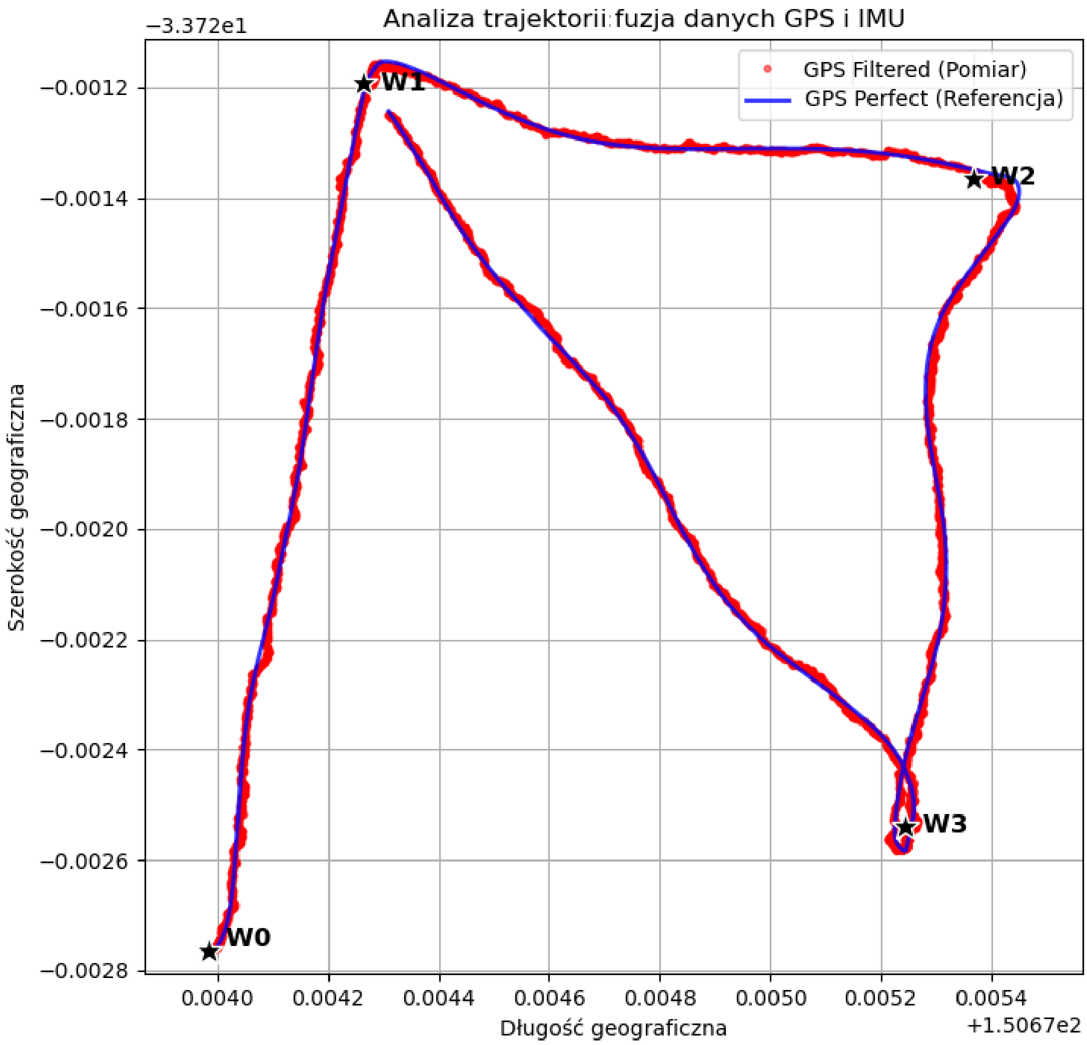

Figure 6.4: Trajectory with points estimated by the Kalman filter.

Metryka	**Oś**	**Surowe dane GPS**	**Fuzja GPS + IMU**
MAE (Śr. bład bezwzgl.)	Lat	$1.34 \times 10^{-5\circ}$ (1.486 m)	$3.77 \times 10^{-6\circ}$ (0.418 m)
	Lon	$1.37 \times 10^{-5\circ}$ (1.268 m)	$4.30 \times 10^{-6\circ}$ (0.398 m)
STD (Odchylenie std.)	Lat	$1.68 \times 10^{-5\circ}$ (1.862 m)	$4.75 \times 10^{-6\circ}$ (0.527 m)
	Lon	$1.72 \times 10^{-5\circ}$ (1.597 m)	$5.44 \times 10^{-6\circ}$ (0.504 m)
Wariancja [deg^2]	Lat	2.82×10^{-10}	2.26×10^{-11}
	Lon	2.97×10^{-10}	2.96×10^{-11}

Table 6.1: Porównanie statystyk błedu pozycjonowania.

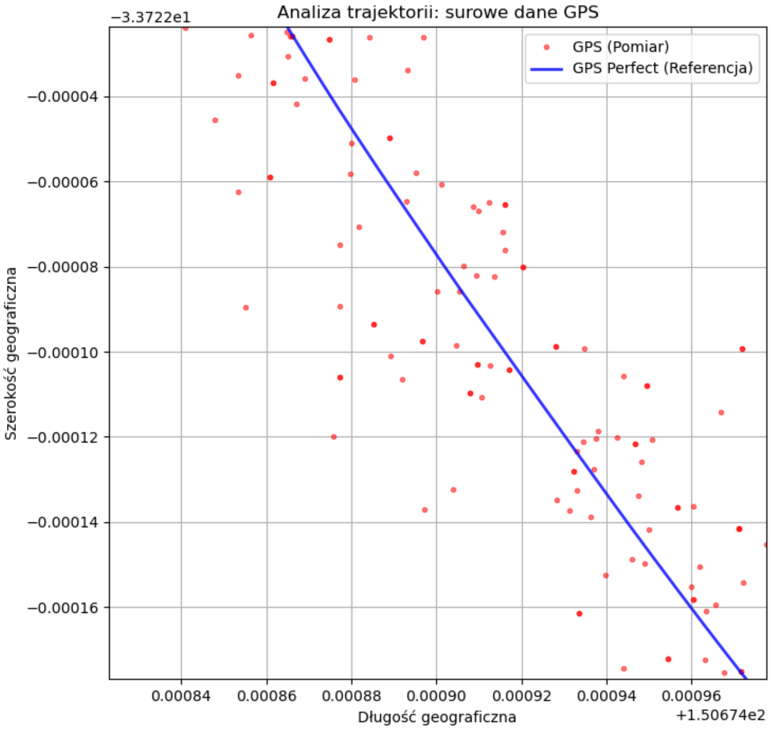

(a) Fragment of the trajectory with raw GPS measurement points.

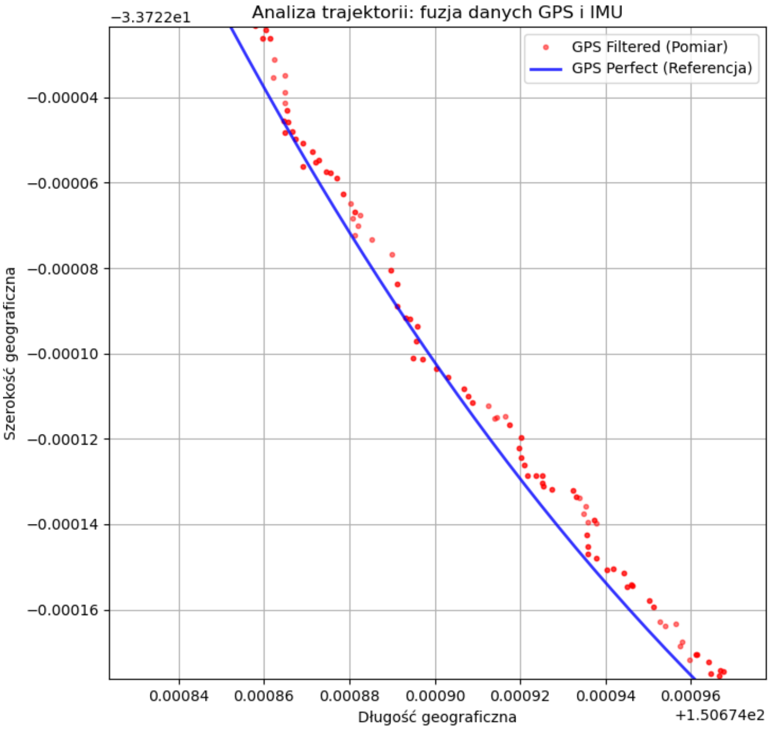

(b) Fragment of the trajectory with points estimated by the Extended Kalman Filter.

Figure 6.5: Magnified trajectories of the WAM-V boat with marked measurements.

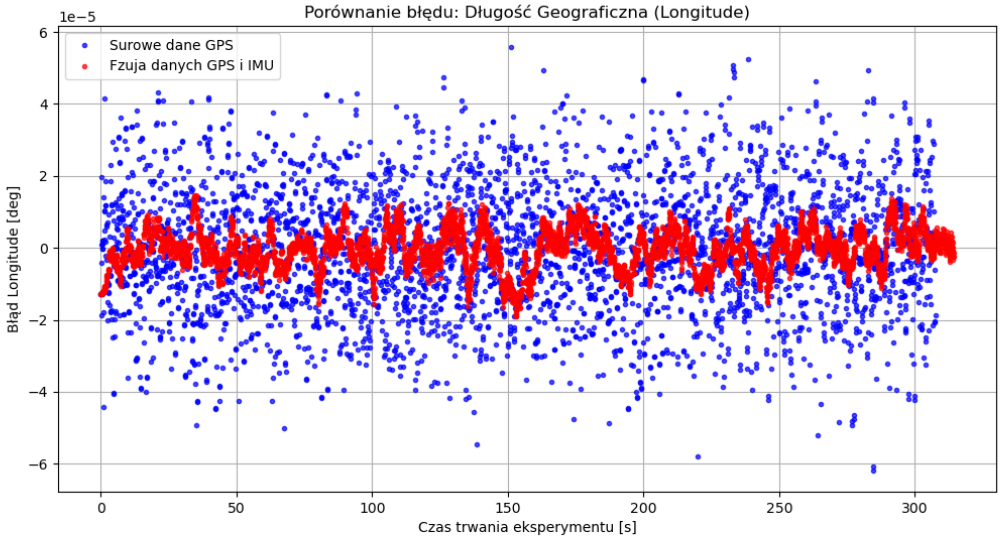

(a) Estimation errors for longitude: raw GPS receiver vs. sensor fusion.

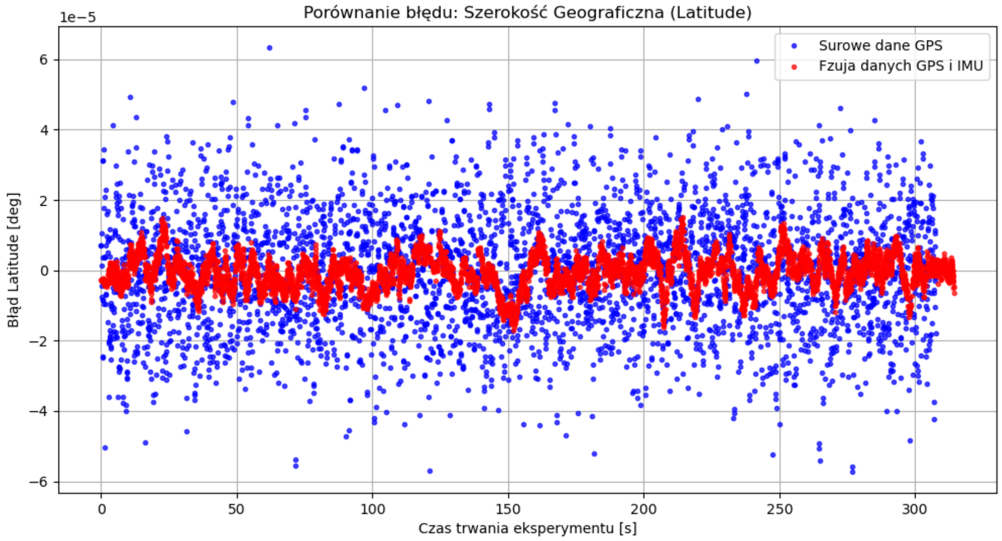

(b) Estimation errors for latitude: raw GPS receiver vs. sensor fusion.

Chapter 7

Physical Tests

7.1 Test Scenario

Identified magnetometer measurement errors, including a constant offset and characteristic non-linearity (discrepancy between the physical rotation angle and the change in the measured value), prevented the full implementation of point-to-point navigation and trajectory tracking algorithms. Consequently, the scope of research was limited to two verification experiments.

The tests were conducted using the "FOKA" boat, constructed by the PWr Solar Boat Team student research club. The testing site was a section of the Oder River near the boulevards of the Wrocław University of Science and Technology (geographic coordinates: 51.106509; 17.061303). The configuration of the unit with an attached safety line is shown in Figure 7.1.

The first experiment aimed to verify the correctness of the azimuth measurement and estimate the magnetometer error. The research procedure involved manual, uniform rotation of the unit around the vertical axis while maintaining a constant horizontal plane. The azimuth signal sampling frequency was 10 Hz.

The second test involved verifying the performance of the heading controller in a closed-loop system. A compass heading setpoint of 130° was adopted; however, due to the sensor's non-linearity, this value did not necessarily coincide with the actual geographic azimuth. A line was attached to the boat to serve as a safety measure and to introduce disturbances (external impulses) once the system reached a steady state. The task of the control system was to maintain the desired heading over a distance of approximately 15 m. A proportional (P) controller with a gain of $K_p = 0.03$ was used in the algorithm. The longitudinal velocity control signal was limited to $v = 0.15$. Data recording also took place at a frequency of 10 Hz. The error of the measured value relative to the setpoint was adopted as the quality indicator.

7.2 Results Analysis

The first stage of the tests revealed significant non-linearity in the magnetometer characteristic, as illustrated in Figure 7.2. The largest discrepancy between the readings and the reference characteristic was observed in the time interval $t \in \langle 10, 25 \rangle$ s, with the error exceeding 50° at the 15th second. Such significant mapping errors disqualify the use of raw sensor data in the control system and indicate the necessity of a calibration process. To increase the clarity of the analysis, the data in the plot were normalized relative to the

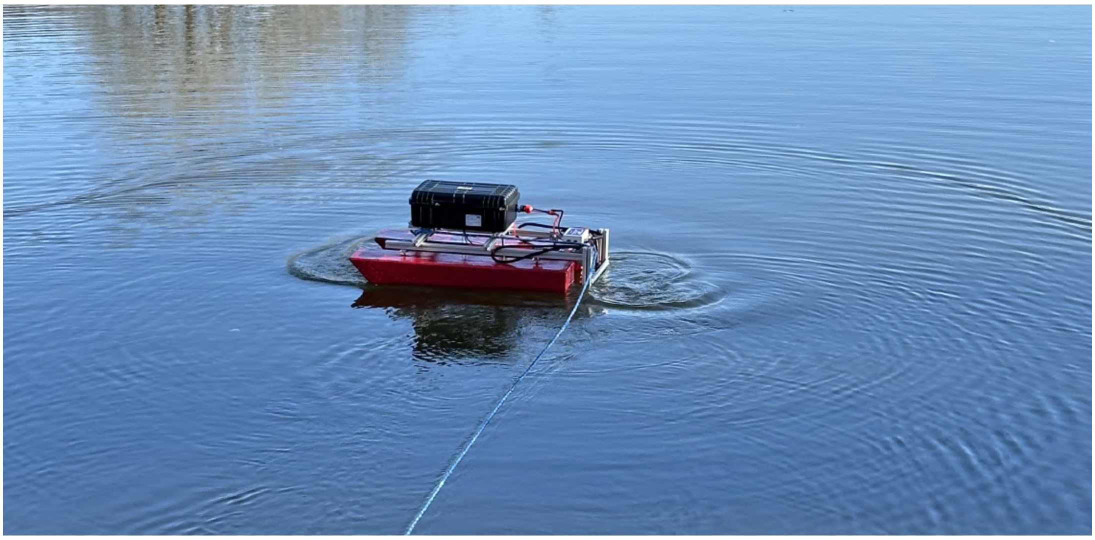

Figure 7.1: Photograph showing the "FOKA" boat with the attached line.

initial orientation of the unit (0°), due to the inability to verify the absolute error relative to magnetic North.

During the second test (Fig. 7.3), the performance of the proportional (P) controller in the heading-keeping task was verified. The system reached the setpoint after 10 s, though full stabilization occurred at the 33rd second of the trial. An external disturbance deliberately introduced at the 34th second (via the tether) caused a heading deviation of approximately 13°, after which the system returned to the steady state within 22 s (at the 55th second of the test). The system response was characterized by a significant overshoot with an initial amplitude of approximately 10°, which, however, allowed for a short rise time, crucial for maneuvering in small water bodies.

A steady-state error of approximately 1° was also observed, which may result from the hydrodynamic asymmetry of the hull or measurement errors. Although the azimuth controller functioned correctly, it should be emphasized that due to the sensor's non-linearity, the recorded angular values are subject to mapping error. To visualize the trend, a 10-point moving average was applied to the plot.

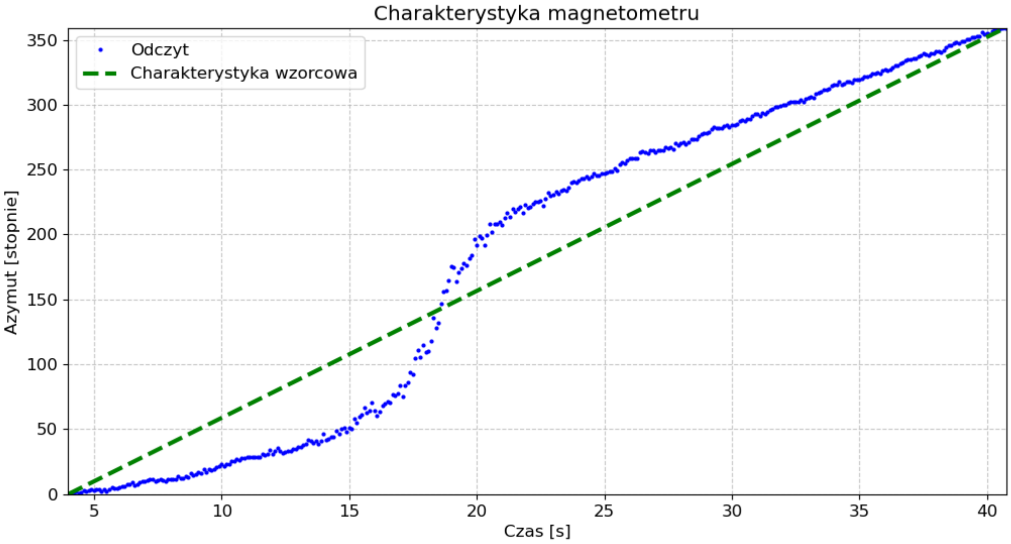

Figure 7.2: Magnetometer characteristic alongside the reference characteristic.

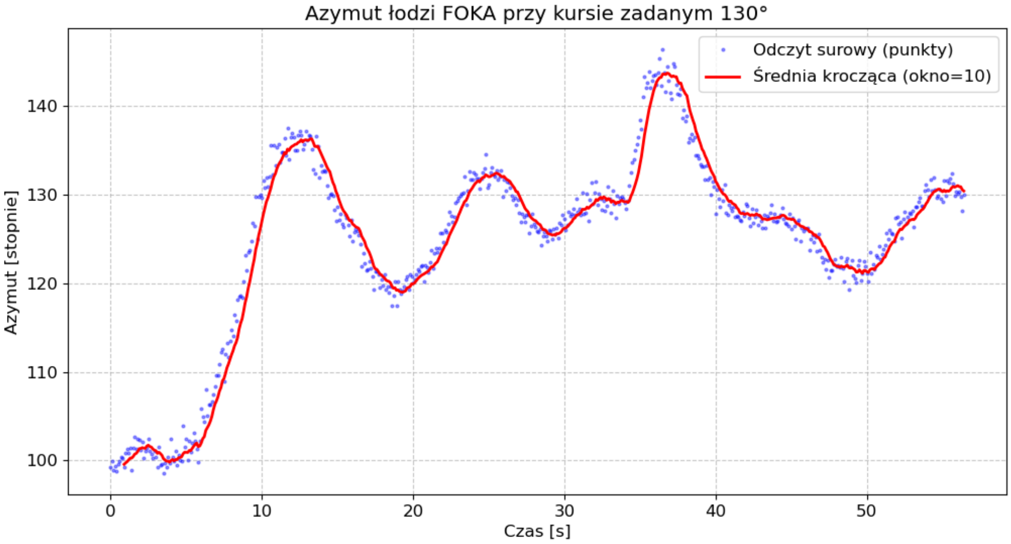

Figure 7.3: Azimuth plot of the "FOKA" boat with a 130° setpoint, including a moving average for better trend visualization.

Chapter 8

Summary

The main objective of this thesis, defined as the proposal, implementation, and verification of control algorithms for a USV-class floating robot, has been achieved. During the literature review, various concepts of unmanned surface vehicles were analyzed, with particular attention paid to differential-drive catamaran designs. Based on this, a mathematical dynamic model of the vessel was developed, which—after adopting appropriate simplifications—was reduced to three degrees of freedom (3 DOF) for planar motion.

The verification of the proposed solutions was carried out in two stages. The first phase consisted of simulation tests performed in the Gazebo Sim software, integrated with the ROS 2 environment.

The test scenarios accounted for environmental disturbances, including varying wind, which allowed for the assessment of the control system's robustness. A key aspect of the research was the analysis of navigation algorithms, categorized into three main groups: classical navigation (based solely on the global frame), dead reckoning (utilizing local measurements), and hybrid navigation. The simulations demonstrated a significant advantage for the hybrid approach. The implementation of sensor fusion using the Extended Kalman Filter (EKF) allowed for an approximately 3.5-fold reduction in positioning error compared to navigation based solely on raw GPS data.

The control layer was implemented by mapping control signals to longitudinal velocity (throttle) and angular velocity (steering) parameters. Given the nature of the task, the throttle value was kept constant during tests to focus on maneuvering precision. Algorithms were developed for two types of tasks: orientation stabilization (point control) and path following. The former was implemented in a feedback loop using a heading controller. Although a PD structure was originally intended, an analysis of measurement noise impact—in both simulation and real-world conditions—necessitated the reduction of the algorithm to a proportional (P) term.

The path-following task was implemented in a cascade structure, where the outer loop was handled by PID and ILOS algorithms.

Simulation results indicated that in the analyzed scenario, the PID controller provided faster stabilization on the desired path compared to the ILOS method.

The final stage involved verification tests conducted on the actual research object—the ”FOKA” robot. The experiments confirmed the design's correctness and the operational safety of the vessel.

Due to identified severe magnetometer nonlinearities, the scope of testing was limited to heading controller verification. Despite sensor imperfections, the P-controller-based system performed correctly, effectively stabilizing the vessel's heading.

Bibliography

[1] Adafruit. *Raspberry Pi 4 Model B Specification.* Dokumentacja techniczna.

[2] C. Aguero, i in. Maritime gazebo - open source buoyancy plugin, 2024. Dostep: 2025-05-01.

[3] ApisQueen. *Propeller Controll Specification.* Dokumentacja techniczna.

[4] ApisQueen. *Under Water Thruster Specification.* Dokumentacja techniczna.

[5] M. Bibuli, W. Caharija, K. Y. Pettersen, G. Bruzzone, M. Caccia, E. Zereik. Ilos guidance: Experiments and tuning. *Proceedings of the 19th IFAC World Congress*, strony 1217–1222, Cape Town, South Africa, 2014.

[6] M. Breivik, V. Hovstein, T. Fossen. Straight-line target tracking for unmanned surface vehicles. *Modeling, Identification and Control (MIC)*, strony 131–149, 10 2008.

[7] G. D. v. d. B. D. Y. R. J.-B. A. D. S. R. S. I. A. N. M. R. P. I. M. A. H. K. A. A. A. M. S. P. A. B. S. A. P. H. M. A. A. N. S. F. B. B. Z. M. M. W. M. Y. L. P. W. Y. M. A. . A. B. Budianto Hakim, Unggul Prasetyo Wibowo. Hominins on sulawesi during the early pleistocene. *nature*, 2025.

[8] W. Caharija. *Integral Line-of-Sight Guidance and Control of Underactuated Marine Vehicles.* Praca doktorska, Norwegian University of Science and Technology (NTNU), Trondheim, Norway, 2014.

[9] Drents Museum. The pesse canoe: The world's oldest boat. `https://drentsmuseum.nl/en/collection/pesse-canoe`.

[10] Euronaval Online 2020. Bezzałogowa łódź protector. https://www.armyrecognition.com/archives/archives-naval-defense/naval-defense-2020/euronaval-online-2020-rafael-presents-its-combat-proven-protector-usv-unmanned-surface-vessel.

[11] T. I. Fossen. *Handbook of Marine Craft Hydrodynamics and Motion Control.* John Wiley & Sons, Chichester, UK, 2011.

[12] T. I. Fossen, M. Breivik, R. Skjetne. Line-of-sight path following of underactuated marine craft. *Proceedings of the 6th IFAC Conference on Manoeuvring and Control of Marine Craft*, strony 211–216, Girona, Spain, 2003.

[13] J. Jin, J. Zhang, D. Liu. Design and verification of heading and velocity coupled nonlinear controller for unmanned surface vehicle. *Sensors*, 18(11), 2018.

[14] A. Kolesińska. Łódź stworzona przez wrocławskich studentów ruszy w rejs po atlantyku. statek passat przeszedł pierwsze testy na odrze. https://gazetawroclawska.pl/lodz-stworzona-przez-wroclawskich-studentow-ruszy-w-rejs-po-atlantyku-statek-passat-przeszedl-pierwsze-testy-na-odrze/ar/c1p2-27651277.

[15] J. Kedzierski. Filtr kalmana - zastosowania w prostych układach sensorycznych, 2007. Dostep: 2025-05-01.

[16] lady ada. *LSM9DS1 Accelerometer + Gyro + Magnetometer 9-DOF Specification*. Adafruit. Dokumentacja techniczna.

[17] C. Marchaj. *Teoria żeglowania: Hydrodynamika kadłuba*. Almapress, Warszawa, 2013.

[18] T. Moore, C. Stache. robot_localization: A ros package for nonlinear state estimation, 2014. Dostep: 2025-05-01.

[19] Ocean Power Technologies. Ocean power technologies - hydrographic applications. https://oceanpowertechnologies.com/solutions/hydrographic/.

[20] Open Robotics. *ros2 Humble Specification*. Dokumentacja techniczna.

[21] A. Piałucha. Kod źródłowy symulacji: Sterowanie jednostka usv w środowisku gazebo. `https://github.com/antpial/thesis_SUV_gazebo`.

[22] C. Saildrone. Saildrone voyager equipped for coastal mapping in the atlantic ocean. https://www.saildrone.com/media-room.

[23] S. Verhagen. The pesse canoe: the oldest boat of the world. *Maritime Archaeology Periodical*.

[24] Waveshare. *L76K GNSS Module Specification*. Dokumentacja techniczna.

[25] C. Widłak. Porównanie wartości cep (circular error probable) obliczonych według różnych zależności podawanych w literaturze. *Biuletyn Wojskowej Akademii Technicznej*, 2010. (Publikacja pogladowa / Techniczna).

[26] S. Wu, H. Ye, W. Liu, X. Yang, Z. Liu, H. Zhang. A ship path tracking control method using a fuzzy control integrated line-of-sight guidance law. *Journal of Marine Science and Engineering*, 2024.